

Atomistic and mean-field estimates of effective stiffness tensor of nanocrystalline materials of cubic symmetry

Katarzyna Kowalczyk-Gajewska*, Marcin Maździarz

Institute of Fundamental Technological Research Polish Academy of Sciences, Warsaw, Poland

Abstract

Anisotropic core-shell model of a nano-grained polycrystal, proposed recently for nanocrystalline copper, is applied to estimate elastic effective properties for a set of crystals of cubic symmetry. Materials selected for analysis differ in the lattice geometry (face-centered cubic vs. body-centered cubic) as well as the value of a Zener factor: a ratio of two shear moduli defining elastic anisotropy of a cubic crystal. The predictions are verified by means of the atomistic simulations. The dependence of the overall bulk and shear moduli on the average grain diameter is analysed. In the mean-field approach the thickness of the shell is specified by the *cutoff radius* of a corresponding atomistic potential, while the grain shell is isotropic and its properties are identified by molecular simulations performed for very small grains with approximately all atoms belonging to the grain boundary zone. It is shown that the core-shell model provides predictions of satisfactory qualitative and quantitative agreement with atomistic simulations. Performed study indicates that the variation of the bulk and shear moduli with the grain size changes qualitatively when the Zener anisotropy factor is smaller or greater than one.

Keywords: Molecular statics, Elasticity, Polycrystal, Effective medium, Cubic symmetry, Core-shell model

1. Introduction

Nanostructured materials (NsM) considered in the present research are bulk solids with a nanometre-scale microstructure and a characteristic dimension smaller than 100 nm [1, 2]. In particular, a class of such materials is analysed that is composed of equiaxed nanometre-sized building blocks - crystallites of the same chemical composition, which differ only by the crystallographic orientation [1]. In the microstructure of nanocrystalline metals two main phases are distinguished: the grain core and the grain boundaries. The impact of grain

*Corresponding author.
E-mail address: kkowalcz@ippt.pan.pl

boundary zone on the effective properties of a bulk polycrystal is the more significant the smaller is a grain size [3, 2]. Usually at the macroscale level the stress-strain response of nanocrystalline metals is governed by the continuum mechanics theory.

Because for a considered category of nanocrystalline materials continuum mechanics description is applicable at the macro-level, the mean-field estimates are still in use for assessing the bulk properties of nanocrystalline metals. In [4] an extensive overview of such estimates available in the literature has been presented. In general, in variance with the coarse-grained polycrystals for which one-phase models can be used, for nano-grained polycrystals two-phase or multi-phase frameworks are formulated. In a nutshell they can be categorized into the following three groups:

- simplified mixture rule-based models [5, 6, 7, 8, 9],
- inclusion-matrix models [10],
- composite sphere / generalized self-consistent-type models [11, 12, 13, 14, 15, 4].

The main difficulty encountered when applying those multi-phase concepts is to properly identify the properties of a grain boundary zone (or zones) and its volume fraction and morphology. Identification of those parameters and validation of the models are usually performed employing the molecular dynamics/statics simulations [16, 17, 18, 2, 19, 20, 4]. Occasionally, full-field FEM analyses are also conducted for this purpose, however, in such a case the refined constitutive description with scale effects is used [21]. The most often outcome of atomistic simulations is that elastic stiffness decreases with a grain size [22, 2, 23]. The two- or multi-phase mean-field approaches reproduce the observed tendency when the stiffness of the grain boundary is smaller than the stiffness of the grain core [11, 15, 2].

Reported research is continuation of the work undertaken in [4]. The aim of the present paper is to verify applicability of a core-shell model proposed therein for estimating the effective elastic stiffness of nanocrystalline metals of cubic symmetry. In particular, the additional assumptions taken in the approach and concerning the properties of a grain boundary zone are checked. Moreover, the possible correlation between the Zener factor - the basic anisotropy parameter in the case of elastic cubic symmetry - and the character of size-dependence of effective properties is analysed.

The next section recalls the construction of the core-shell model starting with the discussion on the spectral form of the elasticity tensor of cubic symmetry and the meaning of a Zener parameter. Section 3 presents the basic elements of atomistic simulations. In Section 4 the results of the atomistic simulations are compared with the predictions of a core-shell model. Dependence of the isotropized overall bulk and shear moduli on the averaged grain diameter is studied. Detailed results of molecular simulations are collected in the Appendix. The paper is closed with conclusions.

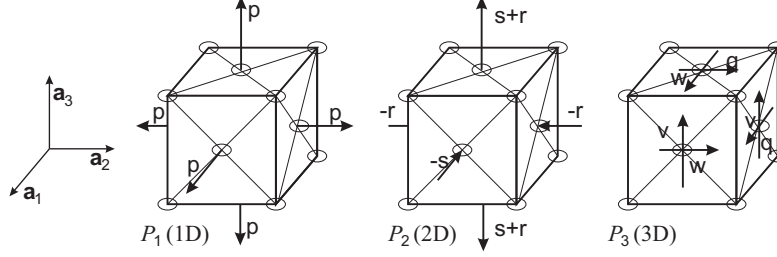


Figure 1: Illustration of eigen-subspaces of the elasticity tensor of cubic symmetry

2. Core-shell model for nanocrystalline materials of cubic symmetry

The anisotropic constitutive relation between the stress $\boldsymbol{\sigma}$ and strain $\boldsymbol{\varepsilon}$ in the grain is

$$\boldsymbol{\sigma} = \mathbb{C}(\phi_c) \cdot \boldsymbol{\varepsilon}, \quad \boldsymbol{\varepsilon} = \mathbb{S}(\phi_c) \cdot \boldsymbol{\sigma}, \quad \mathbb{S}(\phi_c)\mathbb{C}(\phi_c) = \mathbb{I}, \quad (1)$$

where $\mathbb{C}(\phi_c)$, $\mathbb{S}(\phi_c)$ and \mathbb{I} are the fourth order elastic stiffness, compliance and symmetrized identity tensors, respectively. Argument ϕ_c denotes symbolically an orientation of local axes $\{\mathbf{a}_k\}$ with respect to some macroscopic frame $\{\mathbf{e}_k\}$. For crystals of cubic symmetry the local stiffness tensor $\mathbb{C}(\phi_c)$ can be written in the following spectral form [24, 25, 26]

$$\mathbb{C}(\phi^c) = 3K\mathbb{I}^P + 2G_1(\mathbb{K}(\phi^c) - \mathbb{I}^P) + 2G_2(\mathbb{I} - \mathbb{K}(\phi^c)), \quad (2)$$

with

$$\mathbb{I}^P = \frac{1}{3}\mathbf{1} \otimes \mathbf{1} \quad \text{and} \quad \mathbb{K}(\phi_k) = \sum_{k=1}^3 \mathbf{a}_k \otimes \mathbf{a}_k \otimes \mathbf{a}_k \otimes \mathbf{a}_k. \quad (3)$$

$\mathbf{1}$ denotes the second order identity tensor. The material parameters $3K$, $2G_1$ and $2G_2$ are Kelvin moduli which can be expressed by means of the components of the stiffness tensor in the basis of local anisotropy axes $\{\mathbf{a}_k\}$ (see Fig. 1), namely

$$3K = C_{1111} + 2C_{1122}, \quad 2G_1 = C_{1111} - C_{1122}, \quad 2G_2 = 2C_{2323}. \quad (4)$$

Three Kelvin moduli $3K$, $2G_1$ and $2G_2$ correspond to three eigen-subspaces of strain or stress states, which are respectively:

- the one-dimensional space of hydrostatic states,
- the two-dimensional space of deviatoric states with eigen-vectors coaxial with anisotropy axes \mathbf{a}_k ,
- the three-dimensional space of deviatoric states with only shear components in the basis \mathbf{a}_k .

This subspaces are schematically illustrated in Fig. 1. For the states belonging to the respective subspaces the proportionality is observed between stress and strain tensors.

The parameter, proposed as an anisotropy measure for cubic crystals by [27], is defined as

$$\zeta_1 = \frac{C_{1111} - C_{1122}}{2C_{2323}} = \frac{G_1}{G_2}. \quad (5)$$

Note that the condition $\zeta_1 = 1$ is sufficient to ensure elastic isotropy of cubic crystal. The qualitative difference in elastic response is observed for materials with $\zeta_1 > 1$ or $\zeta_1 < 1$. In particular, if $\zeta_1 < 1$ the maximal and minimal directional Young moduli are found for directions $\{001\}$ and $\{111\}$, respectively. A reverse result is obtained if $\zeta_1 > 1$ [28].

In view of the classical micromechanical theories coarse-grained polycrystals are treated as one-phase heterogeneous materials. Their heterogeneous response results from the varying orientation of crystal axes in the polycrystalline representative volume element. Effective properties of the grain aggregate are estimated assuming that local elastic properties are known and then performing a micro-macro transition. The formulas for the standard estimates, such as the Voigt, Reuss, Hashin-Shtrikman or self-consistent one, can be found in [4]. These estimates are not sensitive to the grain size.

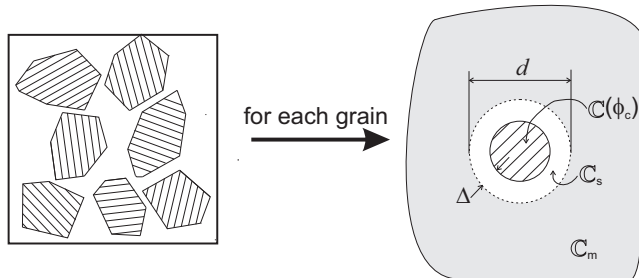


Figure 2: Schematic of the core-shell model of the nanograin polycrystal.

For nanograined polycrystals the concept of one-phase material has to be abandoned in favour of a two- or multi-phase medium. As listed in Section 1 a family of approaches using such concept can be found in the literature. Specifically, in [4] the authors formulated a two-phase model in two variants called *the Mori-Tanaka (MT) and self-consistent (SC) core-shell model*, respectively. As inspired by [11] and [13] an additional phase that forms an *isotropic* coating around the *anisotropic* grain core is introduced. The smaller is the grain this transient zone influences more on the effective properties of polycrystal. Yet another proposal for dealing with interphase layer can be found in [29, 30], formulated in a different context of metal-matrix composite reinforced by nanosized inclusions, in which both inclusion and the matrix have isotropic properties. Extending the proposal by [31], authors assumed the existence of the interphase layer between the inclusion and the matrix. This layer

is assumed to have isotropic properties which vary smoothly with "upward convexity". Note that the schematic configuration considered in the present paper is different: the nanocrystalline material is assumed with anisotropic properties of a grain core and uniform isotropic shell (coating). Such anisotropic composite inclusions constitute the polycrystalline material, which, in general, is also effectively anisotropic. Therefore, the approach presented in the above mentioned papers is not directly applicable in the present context. Nevertheless the core-shell model can be formulated in yet another variant which follows this idea, so that inhomogeneous shell properties can be assumed. However, such variant leads to more complicated formulation, while in the same time establishment of actual variation of shell stiffness using atomistic simulations is not an easy task and the results are debatable [32]. Therefore a respective alternative proposal is only shortly described in Appendix B, demonstrating differences with respect to the original formulation using the example of nanocrystalline copper.

Below basic relations for a core-shell model proposed in [4] are shortly recapitulated. By linearity of the local constitutive law overall relations between the averaged strain $\mathbf{E} = \langle \boldsymbol{\varepsilon} \rangle$ and stress $\boldsymbol{\Sigma} = \langle \boldsymbol{\sigma} \rangle$ in the polycrystalline RVE are:

$$\boldsymbol{\Sigma} = \bar{\mathbf{C}} \cdot \mathbf{E}, \quad \mathbf{E} = \bar{\mathbf{S}} \cdot \boldsymbol{\Sigma}, \quad \bar{\mathbf{S}} \bar{\mathbf{C}} = \mathbb{I}, \quad (6)$$

where $\bar{\mathbf{C}}$ (resp. $\bar{\mathbf{S}}$) is the effective stiffness (resp. compliance) tensor of the polycrystal to be found by the mean-field model. Averaging is defined by the formula $\langle \cdot \rangle = \frac{1}{V} \int_V (\cdot) dV$ and is performed over the representative material volume. The estimates of two-phase model presented in the next section are obtained under the assumption that RVE contains infinite set of orientations of random uniform distribution. In such case the averaging operation $\langle \cdot \rangle$ is replaced by the averaging over the orientation space $\langle \cdot \rangle_{\mathcal{O}}$ and when performed over the fourth order tensor $\mathbb{T}(\phi^c)$ gives [33, 34, 26]

$$\langle \mathbb{T}(\phi_c) \rangle_{\mathcal{O}} = \frac{1}{3} (\mathbf{1} \cdot \mathbb{T}(\phi_c) \cdot \mathbf{1}) \mathbb{I}^P + \frac{1}{5} (\mathbb{I}^D \cdot \mathbb{T}(\phi_c)) \mathbb{I}^D, \quad (7)$$

where \mathbb{I}^P and $\mathbb{I}^D = \mathbb{I} - \mathbb{I}^P$ play a role of the fourth order orthogonal projectors to the hydrostatic and deviatoric subspaces of the second order tensor space, correspondingly. Under such assumption the overall stiffness tensor $\bar{\mathbf{C}}$ is isotropic and specified by

$$\bar{\mathbf{C}} = 3\bar{K}\mathbb{I}^P + 2\bar{G}\mathbb{I}^D,$$

where \bar{K} and \bar{G} are the overall bulk and shear moduli, respectively.

According to the core-shell model formulated in [4] the effective stiffness $\bar{\mathbf{C}}$ is calculated by embedding the coated grain in the infinite medium of the stiffness \mathbf{C}_m and next using the procedure of the double-inclusion model [35], namely

$$\bar{\mathbf{C}}_{CS} = [f_0 \mathbf{C}_s \mathbf{A}_s + (1 - f_0) \langle \mathbf{C}(\phi^c) \mathbf{A}(\phi^c) \rangle_{\mathcal{O}}] [f_0 \mathbf{A}_s + (1 - f_0) \langle \mathbf{A}(\phi^c) \rangle_{\mathcal{O}}]^{-1} \quad (8)$$

where

$$\mathbf{A}(\phi^c) = (\mathbf{C}(\phi^c) + \mathbf{C}_*(\mathbf{C}_m))^{-1} (\mathbf{C}_m + \mathbf{C}_*(\mathbf{C}_m)), \quad (9)$$

$$\mathbb{A}_s = (\mathbb{C}_s + \mathbb{C}_*(\mathbb{C}_m))^{-1}(\mathbb{C}_m + \mathbb{C}_*(\mathbb{C}_m)) \quad (10)$$

and $\mathbb{C}_*(\mathbb{C}_m)$ is the Hill tensor [36] depending on the stiffness \mathbb{C}_m of infinite matrix material and the shape of the coated grain, which is assumed as spherical in the present study. For the MT variant of the core-shell model $\mathbb{C}_m = \mathbb{C}_s$ is assumed (the infinite medium has shell properties), while for the SC variant $\mathbb{C}_m = \bar{\mathbb{C}}_{CS}$ (the infinite medium has the effective properties to be found). In formula (8) f_0 is the volume fraction of the transient zone. Assuming the spherical shape of coated grains and denoting by Δ the coating thickness, f_0 is calculated by the formula

$$f_0 = 1 - \left(1 - \frac{2\Delta}{d}\right)^3, \quad (11)$$

where d is an averaged grain diameter. The parameter Δ introduces the size effect to the model. In [4] it was demonstrated that Δ can be taken as equal to the *cutoff radius* of the atomistic potential valid for the considered metal.

In the same paper, in which nanocrystalline copper was analysed, it was additionally assumed that the shell properties are equal to the zeroth order lower bound for the one-phase polycrystal [37], so that the bulk modulus $K_s = K$ and the shear modulus $G_s = \min\{G_1, G_2\}$. In the present work this constraint is released, so that the isotropic shell properties need to be identified separately.

Note that for a coarse-grained polycrystal ($f_0 \rightarrow 0$) the effective properties $\bar{\mathbb{C}}_{CS/SC}$ approach the self-consistent estimate for a one-phase polycrystal. An estimate of shear modulus related to $\bar{\mathbb{C}}_{CS/MT}$ with arbitrary shell properties $\mathbb{C}_s(K_s, G_s)$ and perfectly random orientation distribution, when $f_0 \rightarrow 0$, approaches the following value

$$\bar{G}_{CS/MT}^\infty = \frac{30G_1G_2(2G_s + K_s) + G_s(2G_1 + 3G_2)(8G_s + 9K_s)}{6(3G_1 + 2G_2)(2G_s + K_s) + 5G_s(8G_s + 9K_s)}. \quad (12)$$

This value is some lower (resp. upper) bound estimate of $\bar{\mathbb{C}}$ if the difference $\mathbb{C}_s - \mathbb{C}(\phi_c)$ is negative (resp. positive) definite for any ϕ_c . For very small grains ($f_0 \rightarrow 1$) the estimates $\bar{\mathbb{C}}_{CS/MT}$ and $\bar{\mathbb{C}}_{CS/SC}$ approach each other and coincide with \mathbb{C}_s .

Since the bulk modulus of a coating K_s can be different from the local bulk modulus of a cubic crystal K also the overall bulk modulus \bar{K} , next to the overall shear modulus \bar{G} , can be affected by a grain size, contrary to the result obtained in [4] where the bulk modulus of a coating was equal to the local one. Note that the latter situation (i.e. $\bar{K} = K$) is always obtained for a one-phase polycrystals of cubic symmetry [38].

3. Computational methods

All atomistic calculations were carried out with the use of the Large-scale Atomic/Molecular Massively Parallel Simulator (LAMMPS) [39], the Embedded Atom Model (EAM) [40, 41], and the molecular statics (MS) method (i.e.

at 0K temperature) [40, 42, 43]. The results obtained were analysed and visualized with the Open Visualization Tool OVITO [44]. The methodology for generating polycrystal samples by the Voronoi tessellation method implemented in the Atoms program [45], their pre-relaxation and numerical simulations was taken directly from [4]. The components of stiffness tensor, of all pre-relaxed structures, \bar{C}_{ijkl} were computed by the stress-strain method with the maximum strain amplitude set to be 10^{-4} [39, 46].

In order to study the effect of the cubic crystal system (face-centered cubic (FCC) vs. body-centered cubic (BCC)), the value of a Zener factor as well as the number and size of grains on mechanical properties of polycrystalline material, eight metals with nine grain sizes each were considered in this work, see the following enumeration I–VIII, Tabs. A.5–A.19 and Fig. 3.

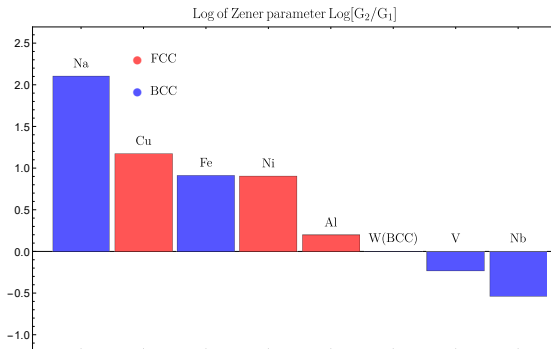


Figure 3: Zener parameter and the lattice geometry for the analysed metals.

There is a generally known problem at the nano level with how to assume local effective material parameters for the interfaces between atomistic layers in the local continuum approach. In such situations the gradation of parameters is sometimes proposed, either step-wise [47] or continuous [29, 30]. The actual properties and their variation along the interphase layer are usually established performing atomistic simulations in a bicrystal configuration [32]. They then depend on the disorientation angle between two grains. In the present study the set of parameters that are representative for an averaged stiffness of an interphase layers between any pair of grain orientations is of interest. Therefore, alternative way of identification of the shell elastic parameters has been adopted. In order to obtain elastic properties for the shells themselves, the size of some generated polycrystal samples was reduced so that the fraction of transient shell atoms approaches unity, $f_0 \rightarrow 1$ (see Eq.(11)). For each material there are two samples with the smallest grain.

I. FCC copper (Cu)

The copper EAM potential parametrized by [48] was utilized. This potential reproduces the copper monocrystal FCC lattice constant $a_{FCC}=3.615 \text{ \AA}$, the cohesive energy $E_c=-3.54 \text{ eV}$, Zener factor $\zeta_1=3.22$, and the elastic constants in crystallographic axes coinciding with Cartesian coordinate system

axes: $C_{1111}=169.88$ GPa, $C_{1122}=122.60$ GPa and $C_{2323}=76.19$ GPa. The characteristics of computational copper samples are listed in the Tab.A.5.

II. FCC aluminum (Al)

The aluminum EAM potential parametrized by [49] was utilized. This potential reproduces the aluminum monocrystal FCC lattice constant $a_{FCC}=4.05$ Å, the cohesive energy $E_c=-3.36$ eV, Zener factor $\zeta_1=1.21$, and the elastic constants in crystallographic axes coinciding with Cartesian coordinate system axes: $C_{1111}=113.80$ GPa, $C_{1122}=61.56$ GPa and $C_{2323}=31.60$ GPa. The characteristics of computational aluminium samples are listed in the Tab.A.7.

III. FCC nickel (Ni)

The nickel EAM potential parametrized by [50] was utilized. This potential reproduces the nickel monocrystal FCC lattice constant $a_{FCC}=3.518$ Å, the cohesive energy $E_c=-4.39$ eV, Zener factor $\zeta_1=2.46$, and the elastic constants in crystallographic axes coinciding with Cartesian coordinate system axes: $C_{1111}=247.0$ GPa, $C_{1122}=147.29$ GPa and $C_{2323}=122.77$ GPa. The characteristics of computational nickel samples are listed in the Tab.A.9.

IV. BCC tungsten (W)

The tungsten EAM potential parametrized by [51] was utilized. This potential reproduces the tungsten monocrystal BCC lattice constant $a_{BCC}=3.14$ Å, the cohesive energy $E_c=-8.9$ eV, Zener factor $\zeta_1=1.00$, and the elastic constants in crystallographic axes coinciding with Cartesian coordinate system axes: $C_{1111}=523.04$ GPa, $C_{1122}=202.19$ GPa and $C_{2323}=160.88$ GPa. The characteristics of computational tungsten samples are listed in the Tab.A.11.

V. BCC iron (Fe)

The iron EAM potential parametrized by [52] was utilized. This potential reproduces the iron monocrystal BCC lattice constant $a_{BCC}=2.87$ Å, the cohesive energy $E_c=-4.29$ eV, Zener factor $\zeta_1=2.48$, and the elastic constants in crystallographic axes coinciding with Cartesian coordinate system axes: $C_{1111}=229.65$ GPa, $C_{1122}=135.50$ GPa and $C_{2323}=116.76$ GPa. The characteristics of computational iron samples are listed in the Tab.A.13.

VI. BCC sodium (Na)

The sodium EAM potential parametrized by [53] was utilized. This potential reproduces the sodium monocrystal BCC lattice constant $a_{BCC}=4.23$ Å, the cohesive energy $E_c=-1.11$ eV, Zener factor $\zeta_1=8.16$, and the elastic constants in crystallographic axes coinciding with Cartesian coordinate system axes: $C_{1111}=8.26$ GPa, $C_{1122}=6.83$ GPa and $C_{2323}=5.84$ GPa. The characteristics of computational sodium samples are listed in the Tab.A.15.

VII. BCC niobium (Nb)

The niobium EAM potential parametrized by [54] was utilized. This potential reproduces the niobium monocrystal BCC lattice constant $a_{BCC}=3.31$ Å, the cohesive energy $E_c=-7.09$ eV, Zener factor $\zeta_1=0.59$, and the elastic constants in crystallographic axes coinciding with Cartesian coordinate system axes: $C_{1111}=233.08$ GPa, $C_{1122}=123.89$ GPa and $C_{2323}=32.13$ GPa.

The characteristics of computational niobium samples are listed in the Tab.A.17.

VIII. BCC vanadium (V)

The vanadium EAM potential parametrized by [55] was utilized. This potential reproduces the vanadium monocrystal BCC lattice constant $a_{BCC}=3.03 \text{ \AA}$, the cohesive energy $E_c=-5.3 \text{ eV}$, Zener factor $\zeta_1=0.79$, and the elastic constants in crystallographic axes coinciding with Cartesian coordinate system axes: $C_{1111}=227.57 \text{ GPa}$, $C_{1122}=119.10 \text{ GPa}$ and $C_{2323}=43.16 \text{ GPa}$. The characteristics of computational vanadium samples are listed in the Tab.A.19.

4. Results

4.1. Results of atomistic simulations

All computational samples of nanocrystalline material subjected to the atomistic simulations are denoted as

$$N_{UC} - N_g - \text{SYS}$$

where N_{UC} is a number of unit cells, N_g - a number of grain orientations and SYS denotes the system of grain distribution, i.e.: BCC or random, see Tables A.5–A.19 included in the Appendix. Similarly to [4] the finite set of N_g orientations has been considered, namely polycrystalline representative volumes composed of grains with 16, 54, 125, 128 or 250 randomly selected orientations, defined in terms of Euler angles, have been analysed. Detailed results, in the form of the full elasticity tensors $\bar{\mathbb{C}}$, derived from molecular simulations of analysed samples for eight cubic metals are listed in the Tables A.6, A.8, A.14, A.16, A.18, A.10, A.12 and A.20, respectively. As it was concluded in the previous study devoted to the nanocrystalline copper the system of grain distribution and the number of orientations in the sample have secondary effect on the magnitude of elastic stiffness, while the primary effect is related to the grain size equivalent to a number of atoms per grain [4].

Selected atomistic computational samples and cohesive energy E_c (eV/atom) are visualized in Fig. 4. As expected, with a decreasing average grain size, the fraction of transient shell atoms in the sample rises. It can be seen that for the samples with a smallest ratio N_{UC}/N_g almost all atoms belong to this zone. As N_{UC}/N_g increases samples can be described as composed of crystalline cores of monocrystal pattern surrounded by amorphous sheaths. It is consistent with the idea of a core-shell model recalled in Sec.2 (see also [56]). As already mentioned, in conjunction with atomistic simulations, the shell thickness Δ can be approximately assessed as equal to *the cutoff radius* of the used potential. The corresponding values of d and f_0 calculated by formula (11) for analysed samples are collected in Tables A.5, A.7, A.9, A.11, A.13, A.15, A.17 and A.19 in Appendix A.

By the assumption that the orientation distribution in the considered samples is random, so it is justified to find the closest isotropic approximation of the calculated elasticity tensors collected in Tables A.6-A.20 in Appendix A.

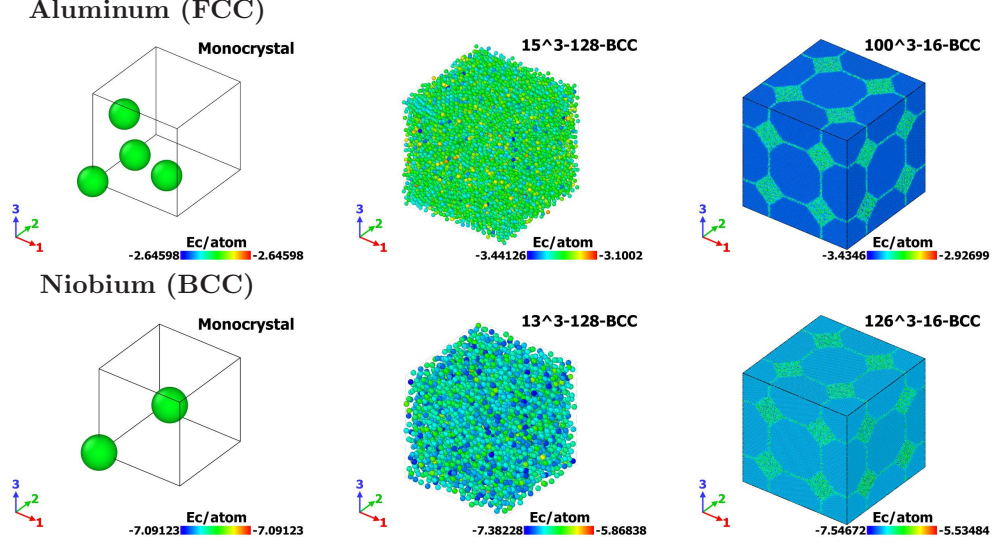


Figure 4: Visualization of selected atomistic computational samples and cohesive energy E_c (eV/atom) for aluminium and niobium.

The closest isotropic approximation $\bar{\mathbb{C}}_{\text{iso}}^{\mathcal{L}}$ of anisotropic $\bar{\mathbb{C}}$ is calculated on the basis of the Log-Euclidean metric [57], namely

$$\bar{\mathbb{C}}_{\text{iso}}^{\mathcal{L}} = \underbrace{\exp\left(\frac{1}{3}\mathbf{1} \cdot \mathbb{Z} \cdot \mathbf{1}\right)}_{=3\bar{K}_{\text{iso}}^{\mathcal{L}}} \mathbb{I}^{\text{P}} + \underbrace{\exp\left(\frac{1}{5}\mathbb{I}^{\text{D}} \cdot \mathbb{Z}\right)}_{=2\bar{G}_{\text{iso}}^{\mathcal{L}}} \mathbb{I}^{\text{D}} \quad \text{where } \mathbb{Z} = \text{Log}\bar{\mathbb{C}}. \quad (13)$$

The two scalars $\bar{K}_{\text{iso}}^{\mathcal{L}}$ and $\bar{G}_{\text{iso}}^{\mathcal{L}}$ will be next compared with the estimates of isotropic bulk and shear moduli obtained by two variants of the core-shell model. The error ζ_2 related to the proposed isotropic approximation is defined by a normalized difference between $\bar{\mathbb{C}}_{\text{iso}}^{\mathcal{L}}$ and the actual $\bar{\mathbb{C}}$. It is defined as [58]

$$\zeta_2 = \frac{\|\text{Log}\bar{\mathbb{C}} - \text{Log}\bar{\mathbb{C}}_{\text{iso}}^{\mathcal{L}}\|}{\|\text{Log}\bar{\mathbb{C}}\|} \times 100\% \geq 0, \quad (14)$$

where $\|\mathbb{A}\| = \sqrt{\mathbb{A} \cdot \mathbb{A}} = \sqrt{A_{ijkl}A_{ijkl}}$ and $\text{Log}\mathbb{A} = \sum_K \log\lambda_L \mathbb{P}_K$ (λ_K - eigenvalues of \mathbb{A} , \mathbb{P}_K - eigenprojectors of \mathbb{A} obtained by its spectral decomposition). Note that ζ_2 can be also used as an anisotropy measure of $\bar{\mathbb{C}}$.

The isotropized bulk and shear moduli obtained by formula (13), together with the anisotropy factor (14), are collected in Tables 1 and 2 for the analysed FCC and BCC cubic metals, respectively. In the tables, in order to facilitate analysis samples are ordered according to the increasing averaged grain size. For each metal the shell elastic parameters: K_s and G_s , were identified as an average value for two samples with f_0 approaching unity. The identified values,

together with the Kelvin moduli of monocrystals and the *cutoff radius* Δ of the applied atomistic potential are collected in Table 3. Metals in the table are ordered according to the decreasing Zener parameter. Interestingly, it can be observed that for the Zener parameter higher than one the identified shell bulk modulus K_s is smaller than the bulk modulus of single crystal K , while a reverse situation takes place for the Zener parameter smaller than one. It is also worth noting that the elastic parameters for the shell for both sample sizes, i.e. averaged over different volumes, are almost identical, which means that resignation from the gradation of elastic parameters within the shell is justified. As it will be shown in the next subsection similar quantitative difference is seen for the shear modulus of shell (grain boundary zone) and the coarse-grained polycrystal. A common trend observed when analysing Tables 1 and 2 is that the elastic moduli increase with a grain size for metals with Zener parameter larger than one (i.e. for sodium, copper, iron and nickel) and decrease with increasing grain size in an opposite case (i.e. for vanadium and niobium). A rule is not clear for tungsten with the Zener parameter approximately equal one for which the bulk modulus decreases, while shear modulus increases with an increasing average grain size. Note that the lattice geometry (FCC vs. BCC) seems not to have such a qualitative influence on the present results. In conclusion the simplifying assumption accepted for nanocrystalline copper in [4] that $K_s = K$ and $G_s = \min\{G_1, G_2\}$ is not valid for other cubic metals.

Table 1: The overall isotropized bulk and shear moduli $\bar{K}_{\text{iso}}^{\mathcal{L}}$ [GPa] and $\bar{G}_{\text{iso}}^{\mathcal{L}}$ [GPa] and anisotropy factor ζ_2 [%] calculated for the effective stiffness tensors resulting from the atomistic simulations for metals of FCC lattice geometry. Samples are ordered according to the increasing average grain size d , while metals according to the decreasing Zener parameter

Sample	Cu			Ni			Al		
	$\bar{K}_{\text{iso}}^{\mathcal{L}}$	$\bar{G}_{\text{iso}}^{\mathcal{L}}$	ζ_2	$\bar{K}_{\text{iso}}^{\mathcal{L}}$	$\bar{G}_{\text{iso}}^{\mathcal{L}}$	ζ_2	$\bar{K}_{\text{iso}}^{\mathcal{L}}$	$\bar{G}_{\text{iso}}^{\mathcal{L}}$	ζ_2
10^3 -128-BCC	134.9	21.99	1.80	91.23	31.44	1.39	74.22	15.51	1.46
15^3 -128-BCC	135.2	22.14	1.44	92.73	32.04	1.10	73.31	15.18	1.10
50^3 -250-BCC	137.2	27.69	1.85	125.7	47.00	1.65	74.84	18.38	3.02
50^3 -128-BCC	137.0	29.50	1.71	133.9	50.71	1.94	75.22	21.65	1.06
50^3 -125-Random	136.6	29.91	2.16	131.5	49.66	2.09	75.20	19.55	2.87
50^3 -54-BCC	136.4	33.65	2.38	142.5	50.70	3.33	76.02	20.85	2.58
50^3 -16-BCC	137.5	36.43	2.86	153.4	59.65	4.23	77.29	24.22	1.91
100^3 -16-BCC	137.9	40.26	2.60	166.2	70.07	2.05	77.69	26.22	0.81

Table 2: The overall isotropized bulk and shear moduli $\bar{K}_{\text{iso}}^{\mathcal{L}}$ [GPa] and $\bar{G}_{\text{iso}}^{\mathcal{L}}$ [GPa] and anisotropy factor ζ_2 [%] calculated for the effective stiffness tensors resulting from the atomistic simulations for metals of BCC lattice geometry. Samples are ordered according to the increasing average grain size d , while metals according to the decreasing Zener parameter

Sample	Na			Fe			W			V			Nb		
	$\bar{K}_{\text{iso}}^{\mathcal{L}}$	$\bar{G}_{\text{iso}}^{\mathcal{L}}$	ζ_2	$\bar{K}_{\text{iso}}^{\mathcal{L}}$	$\bar{G}_{\text{iso}}^{\mathcal{L}}$	ζ_2	$\bar{K}_{\text{iso}}^{\mathcal{L}}$	$\bar{G}_{\text{iso}}^{\mathcal{L}}$	ζ_2	$\bar{K}_{\text{iso}}^{\mathcal{L}}$	$\bar{G}_{\text{iso}}^{\mathcal{L}}$	ζ_2	$\bar{K}_{\text{iso}}^{\mathcal{L}}$	$\bar{G}_{\text{iso}}^{\mathcal{L}}$	ζ_2
X ³ -128-BCC	6.718	1.667	3.72	134.2	42.77	1.00	325.9	84.65	2.14	180.8	65.65	3.31	177.5	44.58	0.52
Y ³ -128-BCC	6.727	1.736	2.45	134.00	40.95	1.23	82.85	327.7	0.84	185.4	65.13	2.60	177.4	45.77	0.37
63 ³ -250-BCC	7.093	1.952	5.39	147.8	54.66	1.04	309.8	109.1	1.88	166.1	51.17	1.63	167.5	40.86	0.77
63 ³ -128-BCC	7.165	2.092	3.65	150.1	57.08	1.23	310.0	117.6	1.34	165.6	51.23	0.97	167.2	40.87	0.64
63 ³ -125-Random	7.157	1.948	7.88	153.1	55.21	2.92	312.1	117.7	0.43	161.4	52.25	2.16	167.7	40.80	0.74
63 ³ -54-BCC	7.234	2.216	8.68	154.3	64.11	1.34	307.2	115.8	3.47	162.6	51.34	1.54	166.2	41.69	0.45
63 ³ -16-BCC	7.265	2.361	10.05	158.1	65.52	2.50	309.1	118.7	2.84	162.9	49.80	0.96	164.3	40.99	0.81
126 ³ -16-BCC	7.293	2.531	10.44	161.8	73.80	2.10	309.2	143.8	0.49	159.0	49.39	0.18	162.2	40.21	1.04

Table 3: Three Kelvin moduli K , G_1 and G_2 of monocrystal samples, identified shell elastic moduli K_s and G_s and *cutoff radius* Δ of the applied atomistic potential for analysed metals. Metals are ordered with a decreasing Zener parameter ζ_1

Metal	K [GPa]	G_1 [GPa]	G_2 [GPa]	ζ_1	K_s [GPa]	G_s [GPa]	Δ [\AA]
Na	7.306	0.7159	5.842	8.16	6.723	1.701	9.2
Cu	138.4	23.64	79.19	3.22	135.0	22.06	5.5
Fe	166.9	47.07	116.8	2.48	134.1	41.86	5.550
Ni	180.5	49.85	122.8	2.46	91.98	31.74	6.0
Al	78.97	26.12	31.59	1.21	73.77	15.35	6.287
W	309.1	160.4	160.9	1.003	326.8	83.75	5.5
V	155.25	54.23	43.15	0.796	183.1	65.39	3.939
Nb	160.3	54.59	32.13	0.588	177.5	45.18	4.75

4.2. Comparison of atomistic and mean-field estimates

The effective elastic properties collected in Tables 1 and 2 are now compared with predictions of a core-shell model in two variants presented in Section 2. In order to calculate estimates infinite number of randomly distributed orientations is assumed, so overall quantities are calculated under the assumption of the overall isotropy. Grains are taken as equal in size and spherical. As already mentioned the shell thickness is assumed to be equal to the *cutoff radius* Δ of the respective EAM atomistic potential for a given metal applied in the molecular simulations, while the shell elastic properties are identified as an average value for two samples with f_0 approaching unity. Figures 5 and 6 present variation of bulk and shear moduli \bar{K} and \bar{G} with a increasing averaged grain diameter as predicted by a core-shell model. Figures concern metals of $\zeta_1 > 1$ and $\zeta_1 \leq 1$, respectively. The results are compared with the outcomes of molecular simulations collected in Tables 1 and 2. In the figures additionally classical estimates of overall shear modulus for coarse-grained polycrystals of cubic constituents obtained by self-consistent (\bar{G}_{SC}) and Reuss (\bar{G}_R) mean-field schemes are shown as reference values. Table 4 includes the collection of all basic classical estimates of overall bulk modulus calculated for the coarse-grained polycrystals of analysed cubic metals with perfectly random distribution of orientations. Let us recall that \bar{G}_{SC} provides the limit of the SC core-shell model for a coarse-grained polycrystal. The corresponding limit value obtained by the MT core-shell model, denoted by $\bar{G}_{CS/MT}^\infty$, is also included in the table. Note that this estimate, contrary to $\bar{G}_{CS/SC}^\infty = \bar{G}_{SC}$, depends on the assumed shell properties. It should be underlined that the respective estimate of the bulk modulus for all the classical averaging schemes is equal to the local bulk modulus K of single crystal.

Table 4: The overall shear modulus $\bar{G}_{\text{iso}}^{\mathcal{L}}$ [GPa] obtained by the Voigt (V), Reuss (R), Hashin-Shtrikman bounds (HS-U, HS-L), self-consistent (SC) estimate and the limit (coarse-grained) value obtained by MT core-shell model for polycrystals with perfectly random orientation distributions and eight cubic metals considered in the present study. Local properties are collected in Table 3.

Metal	R	HS-L	SC	HS-U	V	CS/MT
	[GPa]					
Na	1.512	2.106	2.719	3.053	3.792	2.489
Cu	40.33	46.35	48.60	49.90	55.17	46.12
Fe	73.34	80.03	81.79	82.87	88.91	79.52
Ni	77.46	84.43	86.25	87.37	93.62	82.59
Al	29.15	29.28	29.29	29.29	29.40	29.25
W	160.7	160.7	160.7	160.7	160.7	160.7
V	46.99	47.29	47.30	47.32	47.58	47.35
Nb	38.46	39.71	39.83	40.00	41.11	39.91

It is seen that for all analysed nanocrystalline metals the core-shell model is able to appropriately reproduce, both qualitatively and quantitatively, the

trends observed in the molecular simulations. When comparing two variants of the core-shell model, the estimates obtained by the SC variant are in better agreement with atomistic simulations.

The comparison of core-shell model and atomistic estimates of isotropized Young's modulus $\bar{E}_{\text{iso}}^{\mathcal{L}}$ and Poisson's ratio $\bar{\nu}_{\text{iso}}^{\mathcal{L}}$ are shown in Figs. 7 and 8. Presented values were obtained by applying well-known relations:

$$\bar{E}_{\text{iso}}^{\mathcal{L}} = \frac{9\bar{K}_{\text{iso}}^{\mathcal{L}}\bar{G}_{\text{iso}}^{\mathcal{L}}}{3\bar{K}_{\text{iso}}^{\mathcal{L}} + \bar{G}_{\text{iso}}^{\mathcal{L}}}, \quad \bar{\nu}_{\text{iso}}^{\mathcal{L}} = \frac{3\bar{K}_{\text{iso}}^{\mathcal{L}} - 2\bar{G}_{\text{iso}}^{\mathcal{L}}}{6\bar{K}_{\text{iso}}^{\mathcal{L}} + 2\bar{G}_{\text{iso}}^{\mathcal{L}}}. \quad (15)$$

5. Conclusions

Applicability of a mean-field core-shell model due to [4] for estimation of elastic properties of bulk nanocrystalline cubic metals has been validated. Validation was performed using the results of atomistic simulations since the experimental data for the considered materials are scarce [3, 59, 22, 23]. For an extensive verification of the proposed approach eight metals of cubic symmetry with BCC or FCC lattice geometry and different value of the anisotropy Zener factor (5) were selected (see the collective figure 3). For each metal atomistic simulations have been conducted on eight generated samples of polycrystalline materials with randomly selected orientations. All components of the elastic stiffness tensor are identified by performing six numerical atomistic tests on the generated samples. They vary mainly with respect to the number of atoms per grain, which parameter corresponds to the averaged grain size. In the present analyses an averaged grain diameter takes values between ca. 1 nm to 20 nm.

For the obtained anisotropic stiffness tensor the closest isotropic approximation is found using the Log-Euclidean norm [57]. Next the variation of resulting bulk and shear moduli on a grain size is studied. Interestingly, it is found that the dependence varies quantitatively with the Zener factor: these two stiffness moduli increases (resp. decreases) with the grain size if the Zener factor is higher (resp. lower) than one.

In [4] the two-phase core-shell model was proposed in two variants. The concept follows earlier ideas of [11, 13]. The model is size dependent and the basic length scale parameter is Δ - the thickness of a core coating (see Figure 2), representing the grain boundary zone. This thickness is specified by a *cutoff radius* of the corresponding atomistic potential. Outcomes of present molecular simulations summarized above indicated that the assumptions concerning the stiffness of boundary zone, which were made for nanocrystalline copper in [4], cannot be transferred on other cubic metals. Specifically, it is observed that the bulk modulus may vary with a grain size and the shear modulus of a boundary zone can be equated with none of two modulus of a single crystal. Therefore, in variance with [4], the shell properties are identified separately using the atomistic simulations results for samples with very small grains. When the shell thickness and properties are identified in the described way, obtained

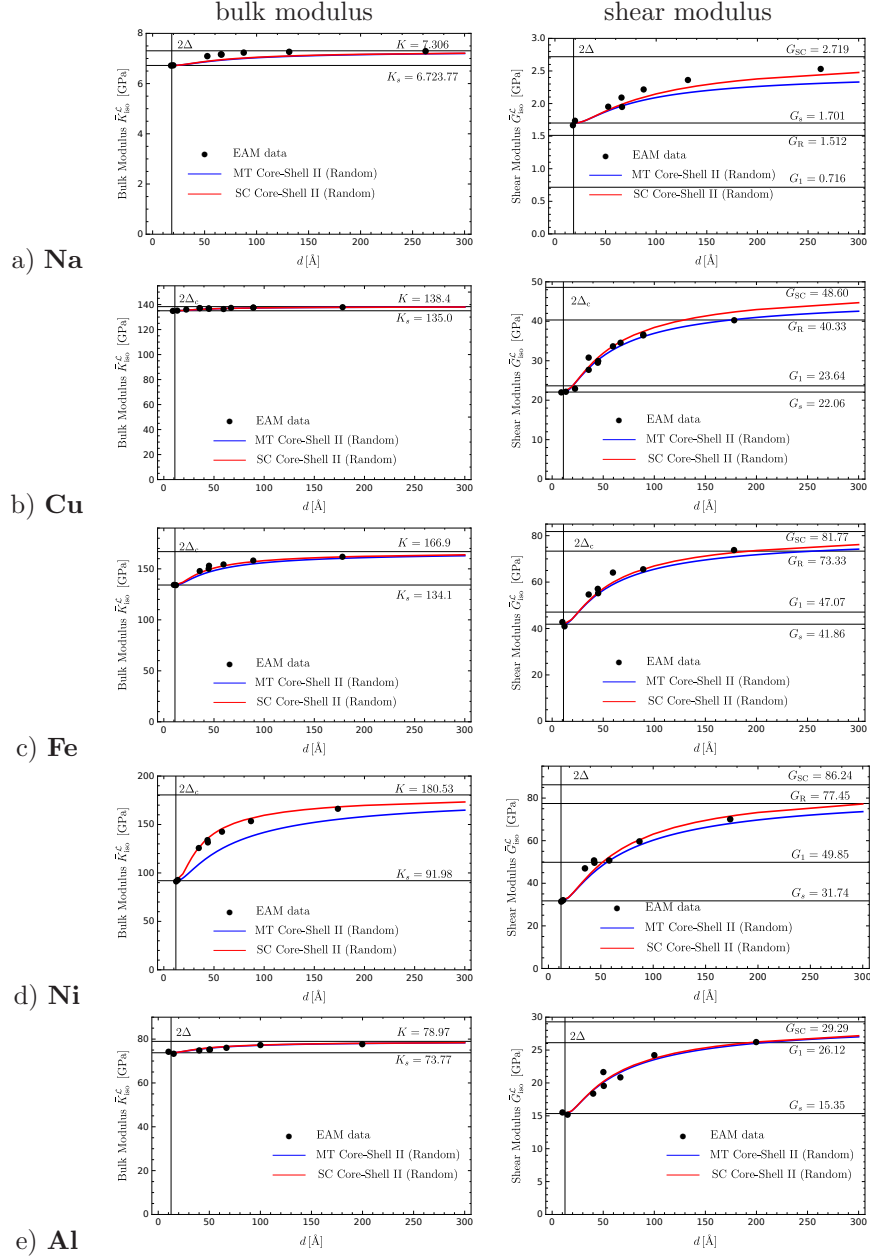


Figure 5: The isotropic bulk and shear moduli $\bar{K}_{iso}^{\mathcal{L}}$ and $\bar{G}_{iso}^{\mathcal{L}}$ as a function of the average grain diameter d by the two variants of the core-shell model - comparison with results of atomistic simulations reported in Tables A.16, A.6, A.14, A.10, A.8 for cubic metals with a Zener parameter $\zeta_1 > 1$: (a) Na, (b) Cu (c) Fe (d) Ni (e) Al.

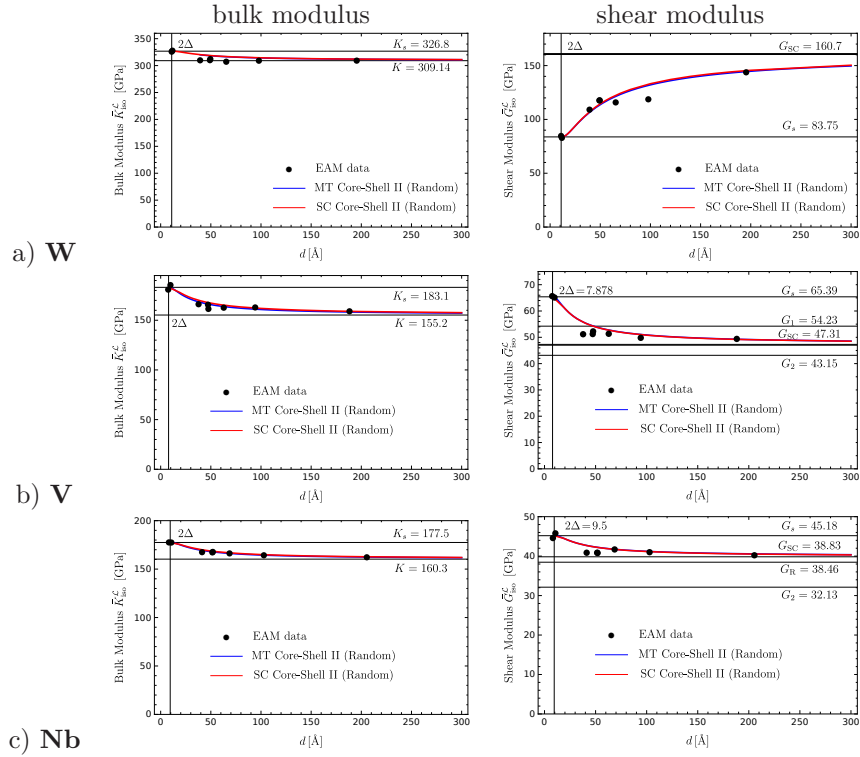


Figure 6: The isotropic bulk and shear moduli $\bar{K}_{\text{iso}}^{\mathcal{L}}$ and $\bar{G}_{\text{iso}}^{\mathcal{L}}$ as a function of the average grain diameter d by the two variants of the core-shell model - comparison with results of atomistic simulations reported in Tables A.12, A.20, A.18 for cubic metals with a Zener parameter $\zeta_1 \leq 1$: (a) W, (b) V (c) Nb.

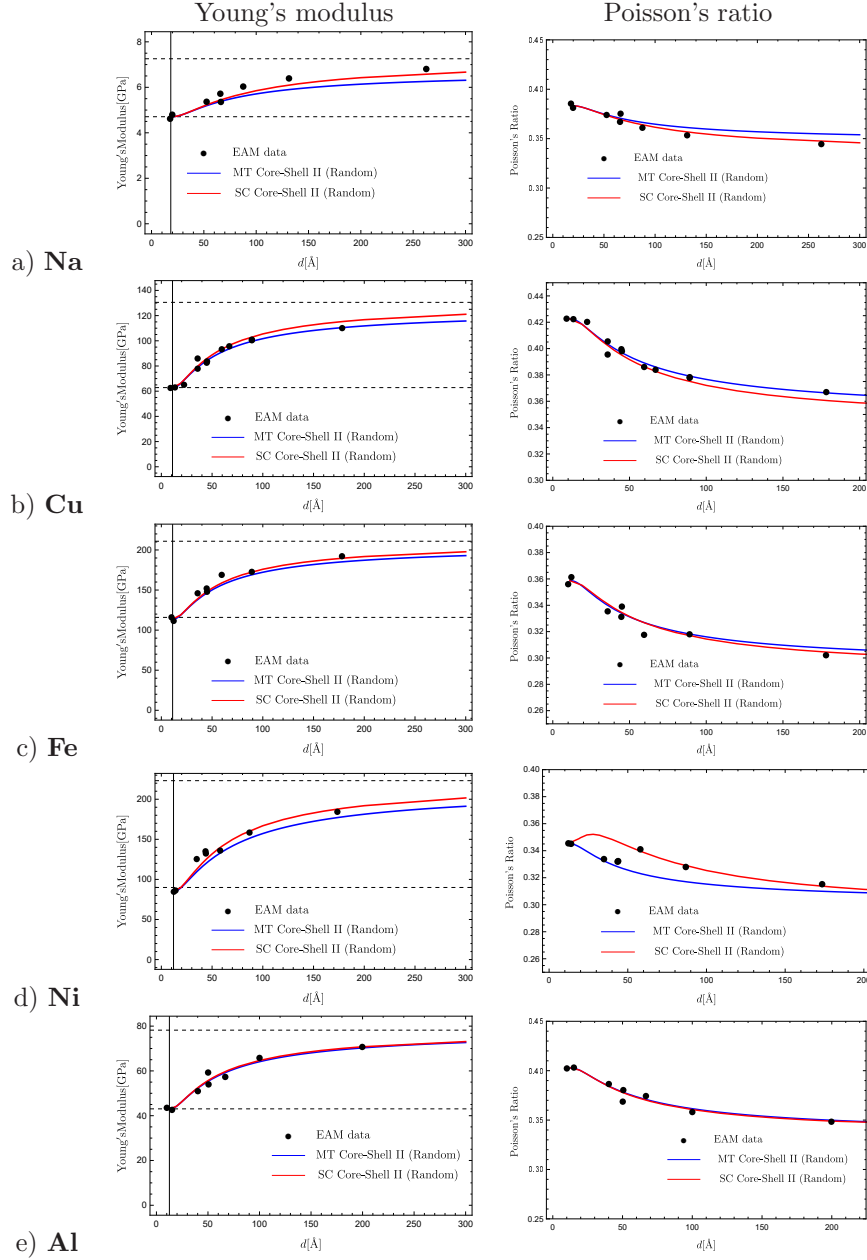


Figure 7: The isotropic Young modulus $\bar{E}_{\text{iso}}^{\mathcal{L}}$ and Poisson's ratio $\bar{\nu}_{\text{iso}}^{\mathcal{L}}$ as a function of the average grain diameter d by the two variants of the core-shell model - comparison with results of atomistic simulations, calculated using Eq. 15, cubic metals with a Zener parameter $\zeta_1 > 1$: (a) Na, (b) Cu (c) Fe (d) Ni (e) Al.

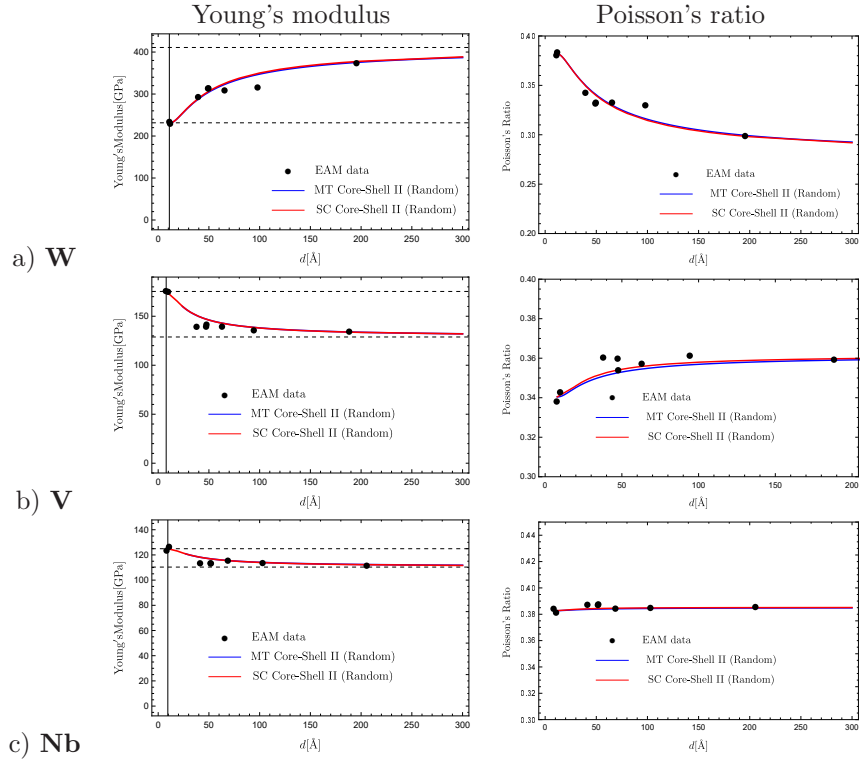


Figure 8: The isotropic Young modulus $\bar{E}_{\text{iso}}^{\mathcal{L}}$ and Poisson's ratio $\bar{\nu}_{\text{iso}}^{\mathcal{L}}$ as a function of the average grain diameter d by the two variants of the core-shell model - comparison with results of atomistic simulations, calculated by Eq. 15, cubic metals with a Zener parameter: $\zeta_1 \leq 1$: (a) W, (b) V (c) Nb.

mean-field estimates are in satisfactory qualitative and quantitative agreement with the results of atomistic simulations for all considered cubic metals.

In the future it will be interesting to confirm experimentally the observed qualitative difference in stiffness related to the Zener parameter, since the present observations strongly rely on validity of the applied atomistic potential and results may change if different EAM potential function is selected for the considered metals. It should be also mentioned that the applied mean-field two-phase model can be extended to estimate a non-linear response of a nano-grained polycrystal and specifically the yield strength as in [11, 13]. Atomistic simulations can be also used to validate such extension of the model.

Appendix A. Detailed results of atomistic simulations

Detailed results of atomistic simulations for nine samples of eight metals are collected in the next subsections. For each metal the first table for a given metal collects quantitative data related to the analysed samples and the second table the calculated 21 components of the anisotropic elasticity tensor for each sample written in the Voigt notation, i.e. in the form of the following 6×6 array:

$$[C_{KL}] = \begin{bmatrix} C_{1111} & C_{1122} & C_{1133} & C_{1123} & C_{1131} & C_{1112} \\ & C_{2222} & C_{2233} & C_{2223} & C_{2231} & C_{2212} \\ & & C_{3333} & C_{3323} & C_{3331} & C_{3312} \\ & & & C_{2323} & C_{2331} & C_{2312} \\ & \text{Sym.} & & & C_{3131} & C_{3112} \\ & & & & & C_{1212} \end{bmatrix}. \quad (\text{A.1})$$

Appendix A.1. Nanocrystalline copper

Table A.5: Copper: Volume (\AA^3), box lengths (\AA), number of atoms, average grain diameter d (\AA), fraction of transient shell atoms f_0 (11), average cohesive energy E_c (eV/atom) of analysed computational samples.

Sample	V	L	No.of atoms	d	f_0	E_c
Monocrystal	47.24	3.615	4			-3.54
10^3 -128-BCC	48634.1	36.50	4016	9.00	1.00	-3.454
15^3 -128-BCC	162305.7	54.52	13430	13.43	0.99	-3.460
50^3 -128-BCC	5985342.9	181.56	499984	44.7	0.57	-3.497
50^3 -16-BCC	5950371.6	181.21	500020	89.2	0.33	-3.516
50^3 -54-BCC	5969399.2	181.40	500058	59.6	0.46	-3.506
50^3 -250-BCC	5997791.1	181.69	500008	35.8	0.67	-3.489
50^3 -125-Random	5985474.7	181.57	499836	45.1	0.57	-3.495
100^3 -16-BCC	47432793	361.99	4000010	178.2	0.17	-3.528

Table A.6: Copper: Elasticity tensors \bar{C} [GPa] of analysed samples (for notation used see Eq. (A.1)).

Monocrystal						10^3 unit cells, 128 grains in BCC system, 4016 atoms (10^3 -128-BCC)					
169.88	122.60	122.60	0	0	0	164.64	118.31	121.89	-0.99	-0.26	0.76
	169.88	122.60	0	0	0		165.65	120.89	-0.26	1.00	0.12
		169.88	0	0	0			161.70	0.98	-0.58	-1.13
			76.19	0	0				23.15	-0.07	1.06
				76.19	0					22.50	-0.43
					76.19						21.02
Sym.						Sym.					
15^3 unit cells, 128 grains in BCC system, 13430 atoms (15^3 -128-BCC)						50^3 unit cells, 128 grains in BCC system, 499984 atoms (50^3 -128-BCC)					
162.44	121.61	121.23	0.18	-0.40	1.24	174.61	116.92	119.13	-0.34	1.11	-1.54
	165.78	118.19	0.17	0.64	-0.66		177.10	117.18	-1.80	1.09	1.17
		166.25	-0.31	0.13	-0.78			174.88	0.18	-0.27	0.08
			21.14	-0.21	0.08				32.96	0.17	-1.63
				22.57	0.29					28.10	1.05
					22.75						29.19
Sym.						Sym.					
50^3 unit cells, 16 grains in BCC system, 500020 atoms (50^3 -16-BCC)						50^3 unit cells, 54 grains in BCC system, 500058 atoms (50^3 -54-BCC)					
182.57	115.48	115.55	-0.65	0.03	-6.23	177.33	116.96	114.38	-1.49	-0.49	-2.32
	182.04	115.56	-1.44	0.09	3.82		179.06	116.59	-1.01	-1.65	2.03
		180.12	1.32	-0.69	2.28			175.49	3.30	3.30	0.30
			38.88	3.44	0.88				36.85	1.42	-0.36
				38.67	-1.52					36.20	-1.05
					40.46						35.09
Sym.						Sym.					
50^3 unit cells, 250 grains in BCC system, 500008 atoms (50^3 -250-BCC)						50^3 unit cells, 125 grains in random system, 499836 atoms (50^3 -125-Random)					
172.29	118.51	120.44	-0.14	0.45	-1.32	176.96	115.67	118.06	3.00	2.65	-2.05
	173.39	119.08	-0.48	0.46	0.35		174.31	118.15	-0.71	-1.01	-0.10
		173.41	1.24	-0.55	0.75			175.02	3.97	1.02	0.04
			28.53	-2.40	-1.77				31.71	2.56	-2.30
				27.57	-1.19					30.66	0.05
					29.23						29.92
Sym.						Sym.					
100^3 unit cells, 16 grains in BCC system, 4000010 atoms (100^3 -16-BCC)											
			186.97	114.79	112.47	-0.88	-0.07	-6.21			
				186.11	113.14	-1.20	1.42	2.40			
					187.21	2.26	-1.08	3.56			
						42.93	2.71	1.77			
							42.50	-1.00			
											44.38
Sym.											

Appendix A.2. Nanocrystalline aluminum

Table A.7: Aluminum: Volume (\AA^3), box lengths (\AA), number of atoms, average grain diameter d (\AA), fraction of transient shell atoms f_0 (11), average cohesive energy E_c (eV/atom) of analysed computational samples.

Sample	V	L	No.of atoms	d	f_0	E_c
Monocrystal	66.43	4.05	4			-3.36
10^3 -128-BCC	68949.29	40.97	3992	10.1	1.00	-3.288
15^3 -128-BCC	231371.86	61.52	13405	15.1	0.99	3.289
50^3 -128-BCC	8449883	203.70	499847	50.1	0.46	-3.325
50^3 -16-BCC	8382312.4	203.11	499935	100.0	0.33	-3.341
50^3 -54-BCC	8419421.3	203.43	500038	66.9	0.58	-3.333
50^3 -250-BCC	8480939.5	203.93	499991	40.2	0.67	-3.318
50^3 -125-Random	8457020.3	203.76	499836	50.6	0.58	-3.323
100^3 -16-BCC	66762145	405.67	4000010	199.7	0.18	-3.350

Table A.8: Aluminum: Elasticity tensors \bar{C} [GPa] of analysed samples (for notation used see Eq. (A.1)).

Monocrystal						10^3 unit cells, 128 grains in BCC system, 3992 atoms (10^3 -128-BCC)					
113.80	61.56	61.56	0	0	0	96.37	64.80	63.67	0.21	-0.20	0.51
	113.80	61.56	0	0	0		93.89	62.94	-0.77	0.95	-0.09
		113.80	0	0	0			95.05	-0.92	0.99	0.48
			31.59	0	0				15.83	0.76	0.36
				31.59	0					15.27	0.01
					31.59						15.32
Sym.						Sym.					
15^3 unit cells, 128 grains in BCC system, 13405 atoms (15^3 -128-BCC)						50^3 unit cells, 128 grains in BCC system, 499847 atoms (50^3 -128-BCC)					
92.59	63.38	63.50	-0.47	0.38	-0.82	103.59	59.47	61.68	0.23	-0.62	0.03
	93.90	62.95	-0.16	0.09	0.56		105.25	61.58	0.09	-1.45	0.36
		93.64	0.76	-0.01	-0.07			102.76	0.17	0.03	0.22
			15.38	-0.25	0.14				21.26	0.69	0.08
				15.15	-0.07					22.16	-0.23
					15.34						22.01
Sym.						Sym.					
50^3 unit cells, 16 grains in BCC system, 499935 atoms (50^3 -16-BCC)						50^3 unit cells, 54 grains in BCC system, 500038 atoms (50^3 -54-BCC)					
108.60	60.66	61.81	-1.94	-0.12	0.40	103.17	61.26	63.36	3.03	1.01	0.59
	107.68	62.68	-0.95	1.07	0.30		104.90	62.18	-0.59	-1.08	-0.41
		109.01	2.78	-0.54	-0.84			102.55	-1.10	1.24	-0.64
			24.35	-0.33	-0.56				19.52	0.64	0.46
				24.46	-0.59					21.13	-1.42
					26.05						23.01
Sym.						Sym.					
50^3 unit cells, 250 grains in BCC system, 499991 atoms (50^3 -250-BCC)						50^3 unit cells, 125 grains in random system, 499836 atoms (50^3 -125-Random)					
98.69	63.30	61.83	0.18	-2.44	-1.32	102.04	60.08	62.42	-0.31	-0.48	-0.94
	97.22	63.77	0.97	0.75	-0.74		101.79	62.67	0.31	0.78	1.27
		99.85	-0.66	0.53	1.30			102.71	1.81	0.15	-0.58
			20.00	-0.08	1.02				20.16	-1.57	-2.17
				19.18	-2.04					19.29	-1.38
					17.86						18.60
Sym.						Sym.					
100^3 unit cells, 16 grains in BCC system, 4000010 atoms (100^3 -16-BCC)											
						111.82	60.96	60.27	-0.24	-0.02	-0.93
							111.27	60.98	-0.01	0.16	0.65
								111.69	0.44	0.07	0.48
									27.25	0.36	-0.08
										26.45	-0.28
											26.61
Sym.						Sym.					

Appendix A.3. Nanocrystalline nickel

Table A.9: Nickel: Volume (\AA^3), box lengths (\AA), number of atoms, average grain diameter d (\AA), fraction of transient shell atoms f_0 (11), average cohesive energy E_c (eV/atom) of analysed computational samples.

Sample	V	L	No.of atoms	d	f_0	E_c
Monocrystal	43.54	3.52	4			-4.39
14^3 -128-BCC	123418.2	49.79	11052	12.1	1.00	-4.261
15^3 -128-BCC	182329.0	56.75	16335	13.0	0.99	-4.264
50^3 -128-BCC	5527341.4	176.80	499984	44.7	0.61	-4.320
50^3 -16-BCC	5491908.5	176.39	500020	89.2	0.35	-4.350
50^3 -54-BCC	5511531.4	176.64	500058	59.5	0.49	-4.335
50^3 -250-BCC	5542256.3	176.97	500008	35.8	0.71	-4.309
50^3 -125-Random	5528944.5	176.81	499836	45.1	0.61	-4.318
100^3 -16-BCC	43749012	352.36	4000010	178.2	0.19	-4.367

Table A.10: Nickel: Elasticity tensors \bar{C} [GPa] of analysed samples (for notation used see Eq. (A.1)).

Monocrystal						14^3 unit cells, 128 grains in BCC system, 11052 atoms (14^3 -128-BCC)					
247.00	147.30	147.30	0	0	0	131.33	68.93	71.44	-1.95	0.12	1.19
	247.00	147.30	0	0	0		135.70	68.75	0.84	0.27	0.24
		247.00	0	0	0			135.85	0.81	-0.75	-1.79
			122.77	0	0				31.09	-1.34	-0.66
				122.77	0					31.40	-0.53
					122.77						30.47
Sym.						Sym.					
16^3 unit cells, 128 grains in BCC system, 16335 atoms (16^3 -128-BCC)						50^3 unit cells, 128 grains in BCC system, 499984 atoms (50^3 -128-BCC)					
136.64	71.04	70.69	-0.91	0.63	0.76	195.44	98.34	103.61	-2.35	-2.03	-0.99
	134.17	71.92	0.88	1.04	0.46		203.37	101.21	-2.48	2.58	2.43
		136.52	0.10	-1.10	-0.46			200.19	2.86	1.35	-3.22
			30.70	-0.66	0.60				53.21	2.76	-2.67
				34.12	-0.03					52.58	-4.71
					31.03						50.49
Sym.						Sym.					
50^3 unit cells, 16 grains in BCC system, 500020 atoms (50^3 -16-BCC)						50^3 unit cells, 54 grains in BCC system, 500058 atoms (50^3 -54-BCC)					
225.72	117.81	117.25	0.11	-4.94	-13.38	215.37	107.09	109.49	-9.02	2.11	-0.67
	226.23	112.46	-2.22	5.98	10.43		204.12	112.09	-2.24	-0.25	-6.54
		234.17	3.80	-0.42	8.47			206.22	11.47	1.01	5.18
			69.93	5.45	5.80				50.53	-3.42	-2.24
				60.36	-8.23					52.64	2.20
					62.76						55.21
Sym.						Sym.					
50^3 unit cells, 250 grains in BCC system, 500008 atoms (50^3 -250-BCC)						50^3 unit cells, 125 grains in random system, 499836 atoms (50^3 -125-Random)					
185.81	95.36	96.31	-4.77	2.21	-0.69	194.81	97.82	96.98	-7.23	-4.55	2.80
	185.41	96.87	-3.02	0.55	1.13		196.70	102.81	0.25	2.80	-3.07
		183.42	1.69	0.15	0.18			196.78	2.24	-0.94	0.70
			53.10	0.12	-1.76				51.82	0.16	-3.44
				46.81	-0.56					53.48	-2.10
					47.30						47.65
Sym.						Sym.					
100^3 unit cells, 16 grains in BCC system, 4000010 atoms (100^3 -16-BCC)											
						250.16	124.20	124.80	-0.23	-0.41	-8.81
							253.06	121.09	-3.20	0.00	3.36
								252.50	3.97	0.11	4.10
									74.18	4.85	0.31
										74.58	-2.05
											75.39
Sym.											

Appendix A.4. Nanocrystalline tungsten

Table A.11: Tungsten: Volume (\AA^3), box lengths (\AA), number of atoms, average grain diameter d (\AA), fraction of transient shell atoms f_0 (11), average cohesive energy E_c (eV/atom) of analysed computational samples.

Sample	V	L	No.of atoms	d	f_0	E_c
Monocrystal	31.06	3.14	2			-8.90
14^3 -128-BCC	87959.41	44.50	5552	10.9	1.00	-8.487
15^3 -128-BCC	107627.75	47.54	6789	11.7	0.99	-8.487
63^3 -128-BCC	7929186	199.41	500269	49.1	0.53	-8.699
63^3 -16-BCC	7861853.7	198.84	500183	98.2	0.30	-8.791
63^3 -54-BCC	7895657.6	199.13	500121	65.46	0.42	-8.743
63^3 -250-BCC	7944642.6	199.54	500207	39.27	0.63	-8.662
63^3 -125-Random	7929410.1	199.41	500118	50.6	0.58	-8.689
126^3 -16-BCC	62509290	396.87	4000817	195.4	0.16	-8.845

Table A.12: Tungsten: Elasticity tensors \bar{C} [GPa] of analysed samples (for notation used see Eq. (A.1)).

Monocrystal						14^3 unit cells, 128 grains in BCC system, 5552 atoms (14^3 -128-BCC)					
523.04	202.19	202.19	0	0	0	431.54	271.43	257.76	-1.95	1.90	23.55
	523.04	202.19	0	0	0		449.18	275.95	0.78	-0.65	-3.31
		523.04	0	0	0			443.80	-1.62	3.22	-2.75
			160.88	0	0				87.17	-2.78	-1.45
	Sym.			160.88	0		Sym.			82.91	-1.46
					160.88						83.47
15^3 unit cells, 128 grains in BCC system, 6789 atoms (15^3 -128-BCC)						63^3 unit cells, 128 grains in BCC system, 500269 atoms (63^3 -128-BCC)					
437.60	272.96	270.05	4.79	2.28	0.18	464.42	238.75	232.20	0.66	-0.11	-4.26
	448.75	273.76	-1.07	3.72	-2.47		463.07	229.66	-4.44	8.18	12.10
		429.72	-3.54	-1.30	-0.25			462.69	3.92	0.72	10.65
			84.64	2.23	-0.90				124.57	2.16	-0.63
	Sym.			81.94	1.24		Sym.			124.30	3.52
					81.76						111.47
63^3 unit cells, 16 grains in BCC system, 500183 atoms (63^3 -16-BCC)						63^3 unit cells, 54 grains in BCC system, 500121 atoms (63^3 -54-BCC)					
478.88	220.10	225.16	-8.55	-5.88	-11.31	474.50	220.26	238.31	-19.69	23.14	-32.94
	463.41	243.55	-0.28	-15.90	9.03		440.61	231.82	-14.25	12.60	-4.48
		462.02	0.55	24.64	-3.03			478.11	11.17	-3.64	0.82
			109.57	16.38	6.06				107.21	13.27	1.73
	Sym.			126.27	0.09		Sym.			109.28	-4.59
					128.30						141.24
63^3 unit cells, 250 grains in BCC system, 500207 atoms (63^3 -250-BCC)						63^3 unit cells, 125 grains in random system, 500118 atoms (63^3 -125-Random)					
452.56	234.89	242.06	-2.32	-4.01	3.08	465.75	235.10	234.81	-1.04	-1.32	1.56
	447.59	240.94	7.36	6.14	9.61		469.61	232.24	-2.52	-1.63	0.82
		453.30	-2.46	17.51	7.22			469.58	5.07	0.20	0.63
			109.92	-3.21	-4.82				118.90	-0.44	0.38
	Sym.			119.58	7.81		Sym.			117.17	-1.80
					107.57						118.33
126^3 unit cells, 16 grains in BCC system, 4000817 atoms (126^3 -16-BCC)											
			493.32	217.42	216.53	-1.06	-1.68	-1.50			
				494.54	216.01	0.96	1.95	0.77			
					494.96	0.67	-1.14	0.04			
						147.42	0.58	0.19			
				Sym.			147.28	0.79			
								146.85			

Appendix A.5. Nanocrystalline iron

Table A.13: Iron: Volume (\AA^3), box lengths (\AA), number of atoms, average grain diameter d (\AA), fraction of transient shell atoms f_0 (11), average cohesive energy E_c (eV/atom) of analysed computational samples.

Sample	V	L	No. of atoms	d	f_0	E_c
Monocrystal	23.54	2.87	2			-4.29
14^3 -128-BCC	67251.15	40.63	5552	10.6	1.00	-4.143
17^3 -128-BCC	119035.24	49.18	9841	12.00	0.99	-4.143
63^3 -128-BCC	5973535.1	181.43	500130	44.46	0.59	-4.217
63^3 -16-BCC	5934590.9	181.04	500095	88.92	0.34	-4.251
63^3 -54-BCC	5954905.6	181.26	500121	59.28	0.47	-4.233
63^3 -250-BCC	5986928.7	181.54	500152	35.57	0.68	-4.203
63^3 -125-Random	5975973.4	181.49	500118	44.81	0.58	-4.214
126^3 -16-BCC	47294569	361.62	4000811	177.83	0.18	-4.269

Table A.14: Iron: Elasticity tensors \bar{C} [GPa] of analysed samples (for notation used see Eq. (A.1)).

Monocrystal						14^3 unit cells, 128 grains in BCC system, 5552 atoms (14^3 -128-BCC)					
229.65	135.50	135.50	0	0	0	188.58	107.73	105.40	-0.35	1.02	-0.42
	229.65	135.50	0	0	0		187.06	106.98	1.15	-0.30	2.04
		229.65	0	0	0			192.44	0.78	0.21	0.11
			116.76	0	0				44.56	0.78	-0.59
				116.76	0					42.36	0.66
					116.76						44.55
Sym.						Sym.					
17^3 unit cells, 128 grains in BCC system, 9841 atoms (17^3 -128-BCC)						63^3 unit cells, 128 grains in BCC system, 500130 atoms (63^3 -128-BCC)					
186.58	106.35	107.00	-0.05	0.34	1.24	223.27	112.99	114.35	-3.22	-0.75	-0.39
	187.66	109.23	1.49	-0.72	1.99		223.38	114.89	-1.65	-0.06	2.64
		186.80	-1.54	0.77	-2.43			219.49	2.36	-0.59	-2.04
			43.17	0.02	-0.05				60.79	-0.04	-0.03
				41.73	-1.78					59.82	-0.08
					40.76						57.48
Sym.						Sym.					
63^3 unit cells, 16 grains in BCC system, 500095 atoms (63^3 -16-BCC)						63^3 unit cells, 54 grains in BCC system, 500121 atoms (63^3 -54-BCC)					
233.60	119.91	115.65	-4.11	0.39	-9.20	235.69	112.66	114.37	-1.63	-1.79	-4.26
	237.17	119.22	-3.89	-1.02	4.84		235.54	114.83	-1.27	-0.61	3.39
		243.01	5.32	1.35	2.16			233.87	3.09	2.20	0.83
			69.99	5.69	0.69				67.86	1.26	-0.49
				67.76	-4.03					66.61	-1.87
					73.41						65.87
Sym.						Sym.					
63^3 unit cells, 250 grains in BCC system, 500152 atoms (63^3 -250-BCC)						63^3 unit cells, 125 grains in random system, 500118 atoms (63^3 -125-Random)					
217.72	113.46	109.90	-0.96	-1.15	-2.63	230.85	126.02	112.78	5.53	-3.55	2.37
	219.30	112.86	0.79	-0.29	0.25		230.04	113.79	7.13	0.84	8.48
		220.87	0.91	1.52	0.90			214.39	3.07	4.98	-1.92
			57.10	-1.87	0.05				57.73	-10.16	2.20
				57.56	-0.05					54.91	-3.31
					51.84						59.32
Sym.						Sym.					
126^3 unit cells, 16 grains in BCC system, 4000811 atoms (126^3 -16-BCC)											
						253.03	116.99	115.26	-0.61	0.77	-10.71
							252.56	116.04	-3.98	1.09	5.68
								254.30	4.72	-1.56	4.28
									77.19	5.09	1.45
										77.93	2.74
											79.34
Sym.						Sym.					

Appendix A.6. Nanocrystalline sodium

Table A.15: Sodium: Volume (\AA^3), box lengths (\AA), number of atoms, average grain diameter d (\AA), fraction of transient shell atoms f_0 (11), average cohesive energy E_c (eV/atom) of analysed computational samples.

Sample	V	L	No.of atoms	d	f_0	E_c
Monocrystal	75.57	4.23	2			-1.111
17^3 -128-BCC	375856.55	72.10	9841	17.77	1.00	-1.092
19^3 -128-BCC	520818.75	80.46	13638	19.81	0.99	-1.092
63^3 -128-BCC	19037348	267.02	500074	65.57	0.63	-1.101
63^3 -16-BCC	18979403	266.73	500100	131.15	0.36	-1.106
63^3 -54-BCC	19013873	266.95	500173	87.43	0.51	-1.104
63^3 -250-BCC	19059847	267.15	500237	52.46	0.73	-1.10
63^3 -125-Random	19038515	267.02	500118	66.09	0.62	-1.101
126^3 -16-BCC	151533591	533.13	4000898	262.29	0.19	-1.108

Table A.16: Sodium: Elasticity tensors \bar{C} [GPa] of analysed samples (for notation used see Eq. (A.1)).

Monocrystal						17^3 unit cells, 128 grains in BCC system, 9841 atoms (17^3 -128-BCC)					
8.26	6.83	6.83	0	0	0	8.86	5.68	5.60	0.00	-0.04	-0.01
	8.26	6.83	0	0	0		8.73	5.72	0.09	0.03	0.05
		8.26	0	0	0			8.87	-0.07	0.02	0.00
			5.84	0	0				1.74	-0.04	-0.02
				5.84	0					1.72	0.02
					5.84						1.75
Sym.						Sym.					
19^3 unit cells, 128 grains in BCC system, 13638 atoms (19^3 -128-BCC)						63^3 unit cells, 128 grains in BCC system, 500074 atoms (63^3 -128-BCC)					
9.08	5.58	5.50	0.04	-0.01	-0.01	9.74	5.71	5.91	0.13	-0.04	0.01
	9.06	5.58	0.01	-0.04	0.02		9.95	5.85	-0.06	-0.04	0.10
		9.09	-0.03	0.04	0.00			9.85	0.13	0.07	-0.07
			1.78	0.03	0.04				2.24	-0.04	-0.05
				1.64	0.03					2.14	-0.02
					1.75						2.08
Sym.						Sym.					
63^3 unit cells, 16 grains in BCC system, 500100 atoms (63^3 -16-BCC)						63^3 unit cells, 54 grains in BCC system, 500173 atoms (63^3 -54-BCC)					
9.93	5.92	5.95	-0.05	0.08	-0.57	9.84	5.74	6.02	-0.17	-0.07	-0.37
	10.12	5.75	-0.17	0.11	0.31		10.01	6.01	-0.09	-0.02	0.15
		10.10	0.22	-0.19	0.25			9.72	0.25	0.15	0.22
			2.56	0.24	0.10				2.57	0.12	-0.04
				2.59	-0.17					2.44	-0.08
					2.73						2.30
Sym.						Sym.					
63^3 unit cells, 250 grains in BCC system, 500237 atoms (63^3 -250-BCC)						63^3 unit cells, 125 grains in random system, 500118 atoms (63^3 -125-Random)					
9.67	5.78	5.83	-0.01	0.00	0.04	9.86	5.77	5.87	-0.16	-0.19	-0.02
	9.61	5.89	-0.06	-0.08	0.01		9.84	5.85	0.06	0.15	0.03
		9.54	0.06	0.24	-0.01			9.72	0.05	0.05	-0.04
			2.11	-0.14	0.03				2.10	-0.24	0.13
				2.16	-0.04					1.69	0.12
					1.78						2.08
Sym.						Sym.					
126^3 unit cells, 16 grains in BCC system, 4000898 atoms (126^3 -16-BCC)											
						10.22	5.85	5.84	-0.14	0.14	-0.64
							10.31	5.69	-0.18	0.08	0.33
								10.34	0.33	-0.22	0.27
									2.78	0.33	0.15
										2.78	-0.22
											2.91
Sym.											

Appendix A.7. Nanocrystalline niobium

Table A.17: Niobium: Volume (\AA^3), box lengths (\AA), number of atoms, average grain diameter d (\AA), fraction of transient shell atoms f_0 (11), average cohesive energy E_c (eV/atom) of analysed computational samples.

Sample	V	L	No. of atoms	d	f_0	E_c
Monocrystal	36.19	3.31	2			-7.091
10^3 -128-BCC	37081.65	33.33	1989	8.21	1.00	-6.897
13^3 -128-BCC	81017.13	43.16	4343	10.65	0.99	-6.895
63^3 -128-BCC	9172528.1	209.32	500256	51.30	0.46	-7.004
63^3 -16-BCC	9115524.1	208.88	500157	102.61	0.25	-7.045
63^3 -54-BCC	9143533.5	209.11	500121	68.41	0.36	-7.024
63^3 -250-BCC	9193627.1	209.49	500192	41.04	0.55	-6.988
63^3 -125-Random	9176933.2	209.34	500118	51.71	0.46	-6.999
126^3 -16-BCC	72671923	417.29	4000874	205.22	0.13	-7.067

Table A.18: Niobium: Elasticity tensors \bar{C} [GPa] of analysed samples (for notation used see Eq. (A.1)).

Monocrystal						10^3 unit cells, 128 grains in BCC system, 1989 atoms (10^3 -128-BCC)					
233.08	123.89	123.89	0	0	0	236.02	148.34	148.06	-1.41	0.23	-0.31
	233.08	123.89	0	0	0		235.85	147.82	-1.47	0.90	0.25
		233.08	0	0	0			237.56	0.60	1.06	-0.04
			32.13	0	0				44.45	-1.06	-0.12
				32.13	0					44.69	0.17
					32.13						45.45
Sym.						Sym.					
13^3 unit cells, 128 grains in BCC system, 4343 atoms (13^3 -128-BCC)						63^3 unit cells, 128 grains in BCC system, 500256 atoms (63^3 -128-BCC)					
239.34	146.48	148.07	0.65	-0.87	0.32	221.13	140.54	139.15	0.98	-0.46	1.45
	237.38	146.20	-0.42	0.96	0.57		220.79	140.95	-0.41	-0.17	0.87
		238.63	0.68	-0.44	0.22			221.93	-1.24	-0.21	0.87
			45.48	-0.29	-0.24				40.81	0.14	-0.39
				45.39	-0.03					40.29	1.07
					46.49						42.28
Sym.						Sym.					
63^3 unit cells, 16 grains in BCC system, 500157 atoms (63^3 -16-BCC)						63^3 unit cells, 54 grains in BCC system, 500121 atoms (63^3 -54-BCC)					
219.76	136.19	137.22	0.13	0.58	1.79	222.33	138.38	138.01	0.05	-0.39	0.20
	220.32	135.74	0.75	-0.10	-0.70		222.32	138.10	0.75	0.42	-0.63
		219.96	-1.49	0.31	-0.99			222.32	-0.34	-0.80	-0.76
			40.69	-1.12	-0.32				40.81	-0.48	-0.15
				41.36	0.26					41.16	0.45
					39.47						42.38
Sym.						Sym.					
63^3 unit cells, 250 grains in BCC system, 500192 atoms (63^3 -250-BCC)						63^3 unit cells, 125 grains in random system, 500118 atoms (63^3 -125-Random)					
219.87	139.55	141.16	1.09	2.55	-0.77	222.57	139.80	140.60	1.37	0.84	-0.52
	223.63	140.01	0.10	0.31	-2.04		222.99	139.96	1.95	0.59	-0.48
		222.48	-0.10	1.88	0.67			223.18	0.04	0.13	0.40
			40.87	0.32	1.20				40.30	1.77	0.50
				41.31	0.15					40.94	0.44
					40.53						40.11
Sym.						Sym.					
126^3 unit cells, 16 grains in BCC system, 4000874 atoms (126^3 -16-BCC)											
						217.40	133.88	135.30	0.30	0.46	2.62
							217.82	134.64	1.25	-0.13	-1.42
								216.78	-1.57	-0.22	-1.20
									39.57	-1.24	-0.28
										40.14	0.25
											38.93
Sym.						Sym.					

Appendix A.8. Nanocrystalline vanadium

Table A.19: Vanadium: Volume (\AA^3), box lengths (\AA), number of atoms, average grain diameter d (\AA), fraction of transient shell atoms f_0 (11), average cohesive energy E_c (eV/atom) of analysed computational samples.

Sample	V	L	No. of atoms	d	f_0	E_c
Monocrystal	27.82	3.03	2			-5.300
10^3 -128-BCC	28264.68	30.45	1990	7.50	1.00	-5.103
13^3 -128-BCC	61984.58	39.57	4357	9.74	0.99	-5.110
63^3 -128-BCC	7042771.7	191.67	500130	47.19	0.42	-5.215
63^3 -16-BCC	7006050.2	191.35	500095	94.22	0.23	-5.255
63^3 -54-BCC	7026628.8	191.54	500121	62.87	0.33	-5.234
63^3 -250-BCC	7057669.1	191.82	500152	37.78	0.50	-5.198
63^3 -125-Random	7047184.1	191.71	500118	47.57	0.42	-5.210
126^3 -16-BCC	55861236	382.26	4000817	188.22	0.23	-5.277

Table A.20: Vanadium: Elasticity tensors \bar{C} [GPa] of analysed samples (for notation used see Eq. (A.1)).

Monocrystal						10^3 unit cells, 128 grains in BCC system, 1990 atoms (10^3 -128-BCC)					
227.57	119.10	119.10	0	0	0	283.79	137.46	148.78	-0.73	-0.16	0.28
	227.57	119.10	0	0	0		224.10	135.56	-17.57	-3.76	-9.65
		227.57	0	0	0			287.03	-0.67	-0.55	1.40
			43.16	0	0				69.01	0.47	-1.12
	Sym.			43.16	0		Sym.			70.04	0.12
					43.16						69.82
13^3 unit cells, 128 grains in BCC system, 4357 atoms (13^3 -128-BCC)						63^3 unit cells, 128 grains in BCC system, 500130 atoms (63^3 -128-BCC)					
259.63	138.40	139.74	-8.38	11.75	10.62	235.38	128.77	129.22	-3.04	-0.75	-0.87
	288.83	142.92	-4.38	5.77	8.32		234.94	134.76	-2.67	-1.61	-0.41
		285.48	-3.57	2.73	5.46			234.90	0.49	-0.33	-2.34
			65.82	2.27	5.63				52.10	-1.00	-1.73
	Sym.			66.06	-4.61		Sym.			50.63	-0.84
					59.31						49.63
63^3 unit cells, 16 grains in BCC system, 500095 atoms (63^3 -16-BCC)						63^3 unit cells, 54 grains in BCC system, 500121 atoms (63^3 -54-BCC)					
228.63	131.16	129.15	-1.43	0.32	-2.57	224.73	128.38	131.94	2.23	-4.74	-3.80
	228.70	128.55	-0.16	1.19	1.26		228.62	128.88	1.80	-0.54	0.70
		230.89	1.24	-0.71	-1.32			232.11	-2.69	1.82	0.96
			48.12	1.36	-0.04				52.36	1.71	0.53
	Sym.			50.15	-2.00		Sym.			54.20	-1.39
					51.27						52.24
63^3 unit cells, 250 grains in BCC system, 500152 atoms (63^3 -250-BCC)						63^3 unit cells, 125 grains in random system, 500118 atoms (63^3 -125-Random)					
240.59	133.04	130.85	-4.09	-1.55	0.91	230.56	125.92	127.74	-1.53	-4.12	-8.51
	232.44	133.58	-4.64	0.00	-0.57		240.11	125.42	-1.89	4.91	3.68
		227.86	-1.03	4.71	-2.22			224.47	-1.92	1.68	-3.04
			48.48	-2.38	-2.77				54.09	-0.67	2.67
	Sym.			53.98	0.16		Sym.			50.29	-2.90
					53.22						53.27
126^3 unit cells, 16 grains in BCC system, 4000817 atoms (126^3 -16-BCC)											
						225.54	126.12	125.77	-0.09	0.20	-0.08
							225.56	125.69	0.21	0.07	-0.01
								224.84	-0.43	0.07	-0.02
									49.60	0.13	3.99
							Sym.		48.69	-0.08	
											49.24

Appendix B. A core-shell model with an inhomogeneous shell properties

In this appendix an alternative variant of a core-shell model for nanocrystalline material, based on the concept introduced in [29], originally proposed for metal-matrix composites with nanosized inclusions, is shortly outlined. Within this variant, first, effective properties of an anisotropic composite grain are established and next the overall properties of polycrystal composed of composite grains are found applying one of the available averaging schemes for the coarse-grained one-phase polycrystalline materials.

In the first step anisotropic grain core is embedded in the interphase (shell) matrix and the effective anisotropic properties of a composite grain are found in the spirit of a differential scheme. Thus, it is assumed that the respective effective properties are known for the shell layer of thickness h and then the layer is increased by dh . Such an approach enables to consider *inhomogeneous* interphase. When the interphase layer is assumed as locally isotropic then the composite inclusion will be of cubic symmetry, inheriting the anisotropy of a grain core. Using the result of [31] the following differential equations are to be solved to find three effective Kelvin moduli (4):

$$\frac{d\hat{C}(r)}{dr} = -\frac{3}{r} \left((\hat{C}(r) - C_s(r)) + \frac{\alpha_s^C(r)}{C_s(r)} (\hat{C}(r) - C_s(r))^2 \right) \quad (\text{B.1})$$

where $\hat{C}(r)$ stands subsequently for $\hat{K}(r)$, $\hat{G}_1(r)$, $\hat{G}_2(r)$, function $C_s(r)$ for $K_s(r)$, $G_{1s}(r) = G_{2s}(r) = G_s(r)$, respectively, and

$$\alpha_s^K(r) = \frac{1 + \nu_s(r)}{3(1 - \nu_s(r))}, \quad \alpha_s^{G_1}(r) = \alpha_s^{G_2}(r) = \alpha_s^G(r) = \frac{8 - 10\nu_s(r)}{15(1 - \nu_s(r))}$$

where $\nu_s(r)$ is local Poisson's ratio of the shell, which is the function of the shell bulk and shear moduli $K_s(r)$ and $G_s(r)$ according to the formula (15)₂. Differential equations (B.1) are solved with initial conditions $\hat{K}(r_0) = K$, $\hat{G}_1(r_0) = G_1$ and $\hat{G}_2(r_0) = G_2$ (r_0 is a radius of the grain core). The effective Kelvin moduli of a composite grain are then calculated as $\hat{K}_\Delta = \hat{K}(r_0 + \Delta)$, $\hat{G}_{1\Delta} = \hat{G}_1(r_0 + \Delta)$ and $\hat{G}_{2\Delta} = \hat{G}_2(r_0 + \Delta)$. Finally, in the second step, in order to obtain the effective elastic stiffness of a nanocrystalline material, the obtained values are used in place of local properties of the grain within one of the averaging schemes developed for a one phase coarse-grained polycrystals (see Table A.5 in [4]). In this appendix the Hashin-Shtrikman lower bound is used.

Let us now shortly assess the predictive capabilities of this alternative approach on the example of nanocrystalline copper. As already discussed identification of functions $K_s(r)$ and $G_s(r)$ by means of atomistic simulations is not a trivial task. Here, in this preliminary study, following the work by [29] the ad-hoc relation, ensuring smooth variation in accordance with results of [32], is proposed

$$C_s(r) = C_s \left(1 + (\mu - 1) \exp \left(-\frac{b}{\Delta} (r - r_0) \right) \right), \quad (\text{B.2})$$

in which C_s are K_s or G_s from Table 3. In Fig. B.9a the variation the shell shear modulus $G_s(r)$ is presented for varying value of μ and $b = 5$. Note that the assumed form ensures constant Poisson's ratio ν_s along the shell. Using this relation three differential equations specified by Eq. (B.1) have been solved numerically using Wolfram Mathematica. The resulting effective shear modulus of nanocrystalline copper with perfectly random distribution of composite grain orientations, estimated by means of the Hashin-Shtrikman lower bound, is shown in Fig. B.9b. It is worth mentioning that equations (B.1) can be solved analytically for $C_s(r) = C_s$ (equivalent to $\mu = 1$ in Eq. B.2). Effective Kelvin moduli of a composite grain of a diameter d (see Fig. 2) are then given by a closed-form formula,

$$\hat{C}_\Delta = C_s \left(1 + \frac{(C - C_s)(1 - 2\Delta/d)^3}{C_s + \alpha_s^C(C - C_s)(1 - (1 - 2\Delta/d)^3)} \right)$$

Fig. B.9b demonstrates that for constant shell moduli the shear modulus predicted by the alternative variant of core-shell model (SK) are very close to the MT variant. When an inhomogeneous shell is assumed ($\mu \neq 1$), the highest differences between the variants are obviously seen for small grains. As compared to the data obtained by atomistic simulations, good predictions of the SK variant are seen for smaller values of μ in relation (B.2). Nevertheless the improvement of predictions as compared to MT and SC variant is not readily seen. It should be stressed that MT and SC variants, as compared to the alternative model with an inhomogeneous interphase, have the advantage of being simpler (e.g. they do not require numerical integration). They are specified by closed-form formulas with less uncertainty stemming from the applied variation of shell properties.

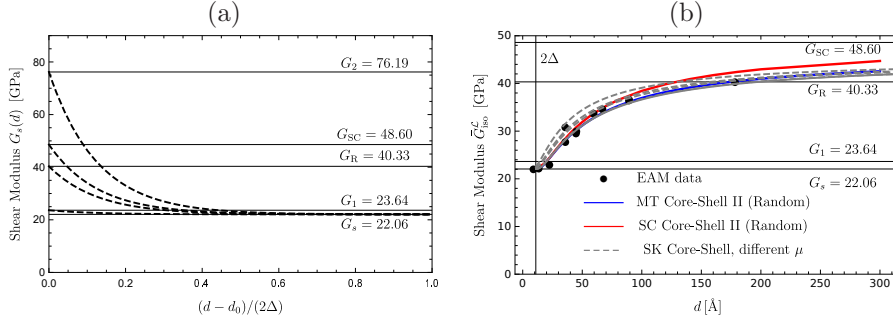


Figure B.9: (a) Assumed variation of the shear modulus $G_s(r)$ along the coating thickness (see Eq. B.2), (b) the isotropic shear modulus of nanocrystalline copper (Cu) as a function of the grain diameter by the differential variant (SK) of core-shell model with shell properties varying according to the formula (B.2) ($b = 5$ and $\mu = G_2/G_s, G_{SC}/G_s, G_R/G_s, G_1/G_s, 1$) - comparison with results of atomistic simulations and estimates of MT and SC variant of core-shell model with a uniform shell properties.

References

References

- [1] H. Gleiter, Nanostructured materials: basic concepts and microstructure, *Acta Materialia* 48 (1) (2000) 1 – 29. doi:10.1016/S1359-6454(99)00285-2.
- [2] G.-J. J. Gao, Y.-J. Wang, S. Ogata, Studying the elastic properties of nanocrystalline copper using a model of randomly packed uniform grains, *Computational Materials Science* 79 (2013) 56 – 62. doi:10.1016/j.commatsci.2013.05.053.
- [3] P. Sanders, J. Eastman, J. Weertman, Elastic and tensile behavior of nanocrystalline copper and palladium, *Acta Materialia* 45 (10) (1997) 4019 – 4025. doi:10.1016/S1359-6454(97)00092-X.
- [4] K. Kowalczyk-Gajewska, M. Maździarz, Atomistic and mean-field estimates of effective stiffness tensor of nanocrystalline copper, *International Journal of Engineering Science* 129 (2018) 47 – 62. doi:10.1016/j.ijengsci.2018.04.004.
- [5] J. Carsley, J. Ning, W. Milligan, S. Hackney, E. Aifantis, A simple, mixtures-based model for the grain size dependence of strength in nanophase metals, *Nanostructured Materials* 5 (4) (1995) 441 – 448. doi:10.1016/0965-9773(95)00257-F.
- [6] H. S. Kim, M. B. Bush, The effects of grain size and porosity on the elastic modulus of nanocrystalline materials, *Nanostructured Materials* 11 (3) (1999) 361 – 367. doi:10.1016/S0965-9773(99)00052-5.
- [7] D. J. Benson, H.-H. Fu, M. A. Meyers, On the effect of grain size on yield stress: extension into nanocrystalline domain, *Materials Science and Engineering: A* 319321 (2001) 854 – 861. doi:10.1016/S0921-5093(00)02029-3.
- [8] X. Qing, G. Xingming, The scale effect on the yield strength of nanocrystalline materials, *International Journal of Solids and Structures* 43 (2526) (2006) 7793 – 7799. doi:10.1016/j.ijsolstr.2006.04.015.
- [9] J. Zhou, Y. Li, R. Zhu, Z. Zhang, The grain size and porosity dependent elastic moduli and yield strength of nanocrystalline ceramics, *Materials Science and Engineering: A* 445446 (2007) 717 – 724. doi:10.1016/j.msea.2006.10.005.
- [10] P. Sharma, S. Ganti, On the grain-size-dependent elastic modulus of nanocrystalline materials with and without grain-boundary sliding, *Journal of Materials Research* 18 (8) (2003) 18231826. doi:10.1557/JMR.2003.0253.

- [11] B. Jiang, G. Weng, A generalized self-consistent polycrystal model for the yield strength of nanocrystalline materials, *Journal of the Mechanics and Physics of Solids* 52 (5) (2004) 1125 – 1149. doi:10.1016/j.jmps.2003.09.002.
- [12] C. Q. Chen, Y. Shi, Y. S. Zhang, J. Zhu, Y. J. Yan, Size dependence of young’s modulus in zno nanowires, *Phys. Rev. Lett.* 96 (2006) 075505. doi:10.1103/PhysRevLett.96.075505.
- [13] L. Capolungo, M. Cherkaoui, J. Qu, On the elastic-viscoplastic behavior of nanocrystalline materials, *Int. J. Plasticity* 23 (2007) 561–591. doi:10.1016/j.ijplas.2006.05.003.
- [14] S. Mercier, A. Molinari, Y. Estrin, Grain size dependence of strength of nanocrystalline materials as exemplified by copper: an elastic-viscoplastic modelling approach, *Journal of Materials Science* 42 (5) (2007) 1455–1465. doi:10.1007/s10853-006-0670-y.
- [15] S. Ramtani, H. Bui, G. Dirras, A revisited generalized self-consistent polycrystal model following an incremental small strain formulation and including grain-size distribution effect, *International Journal of Engineering Science* 47 (4) (2009) 537 – 553. doi:10.1016/j.ijengsci.2008.09.005.
- [16] J. Schiøtz, T. Vegge, F. D. Di Tolla, K. W. Jacobsen, Atomic-scale simulations of the mechanical deformation of nanocrystalline metals, *Phys. Rev. B* 60 (1999) 11971–11983. doi:10.1103/PhysRevB.60.11971.
- [17] W.-J. Chang, Molecular-dynamics study of mechanical properties of nanoscale copper with vacancies under static and cyclic loading, *Microelectronic Engineering* 65 (12) (2003) 239 – 246. doi:10.1016/S0167-9317(02)00887-0.
- [18] Y. Choi, Y. Park, S. Hyun, Mechanical properties of nanocrystalline copper under thermal load, *Physics Letters A* 376 (5) (2012) 758 – 762. doi:10.1016/j.physleta.2011.12.027.
- [19] B. Mortazavi, G. Cuniberti, Atomistic modeling of mechanical properties of polycrystalline graphene, *Nanotechnology* 25 (21) (2014) 215704. doi:10.1088/0957-4484/25/21/215704.
- [20] T.-H. Fang, C.-C. Huang, T.-C. Chiang, Effects of grain size and temperature on mechanical response of nanocrystalline copper, *Materials Science and Engineering: A* 671 (2016) 1 – 6. doi:10.1016/j.msea.2016.06.042.
- [21] T.-Y. Kim, J. E. Dolbow, E. Fried, Numerical study of the grain-size dependent Youngs modulus and Poissons ratio of bulk nanocrystalline materials, *International Journal of Solids and Structures* 49 (26) (2012) 3942 – 3952. doi:10.1016/j.ijsolstr.2012.08.023.

- [22] S.-J. Zhao, K. Albe, H. Hahn, Grain size dependence of the bulk modulus of nanocrystalline nickel, *Scripta Materialia* 55 (5) (2006) 473 – 476. doi:10.1016/j.scriptamat.2006.04.043.
- [23] W. Xu, L. P. Dvila, Size dependence of elastic mechanical properties of nanocrystalline aluminum, *Materials Science and Engineering: A* 692 (2017) 90 – 94. doi:10.1016/j.msea.2017.03.065.
- [24] L. J. Walpole, *Advances in Applied Mechanics*, Vol. 21, 1981, Ch. Elastic Behavior of Composite Metaterials: Theoretical Foundations, pp. 169–236. doi:10.1016/S0065-2156(08)70332-6.
- [25] J. Rychlewski, Unconventional approach to linear elasticity, *Arch. Mech.* 47 (2) (1995) 149–171.
- [26] K. Kowalczyk-Gajewska, Bounds and self-consistent estimates of overall properties for random polycrystals described by linear constitutive laws., *Arch. Mech.* 61(6) (2009) 475–503, <http://am.ippt.pan.pl/am/article/view/v61p475>.
- [27] C. Zener, *Elasticity and Anelasticity of Metals*, University of Chicago Press, 1948.
- [28] J. Ostrowska-Maciejewska, J. Rychlewski, Generalized proper states for anisotropic elastic materials, *Arch. Mech.* 53 (4-5) (2001) 501–518.
- [29] I. Sevostianov, M. Kachanov, Homogenization of a Nanoparticle with Graded Interface, *International Journal of Fracture* 139 (1) (2006) 121–127. doi:10.1007/s10704-006-8369-2.
- [30] I. Sevostianov, M. Kachanov, Effect of interphase layers on the overall elastic and conductive properties of matrix composites. Applications to nanosize inclusion, *International Journal of Solids and Structures* 44 (3) (2007) 1304 – 1315. doi:10.1016/j.ijsolstr.2006.06.020.
- [31] L. Shen, J. Li, Effective elastic moduli of composites reinforced by particle or fiber with an inhomogeneous interphase, *International Journal of Solids and Structures* 40 (6) (2003) 1393 – 1409. doi:10.1016/S0020-7683(02)00659-5.
- [32] M. D. Kluge, D. Wolf, J. F. Lutsko, S. R. Phillpot, Formalism for the calculation of local elastic constants at grain boundaries by means of atomistic simulation, *Journal of Applied Physics* 67 (5) (1990) 2370–2379. doi:10.1063/1.345533.
- [33] S. Forte, M. Vianello, Symmetry classes for elasticity tensors, *J. Elasticity* 43 (1996) 81–108. doi:10.1007/BF00042505.
- [34] J. Rychlewski, Elastic waves under unusual anisotropy, *J. Mech. Phys. Solids* 49 (2001) 2651–2666. doi:10.1016/S0022-5096(01)00083-7.

- [35] M. Hori, S. Nemat-Nasser, Double-inclusion model and overall moduli of multi-phase composites, *Mech. Mater.* 14 (1993) 189–206. doi:10.1016/0167-6636(93)90066-Z.
- [36] R. Hill, Continuum micro-mechanics of elastoplastic polycrystals, *J. Mech. Phys. Solids* 13 (1965) 89–101. doi:10.1016/0022-5096(65)90023-2.
- [37] J. Nadeau, M. Ferrari, On optimal zeroth-order bounds with application to Hashin–Shtrikman bounds and anisotropy parameters, *Int. J. Solids Structures* 38 (2001) 7945–7965. doi:10.1016/S0020-7683(00)00393-0.
- [38] L. Walpole, The stress-strain law of a textured aggregate of cubic crystals, *Journal of the Mechanics and Physics of Solids* 33 (4) (1985) 363 – 370. doi:10.1016/0022-5096(85)90034-1.
- [39] S. Plimpton, Fast Parallel Algorithms for Short-Range Molecular Dynamics, *Journal of Computational Physics* 117 (1) (1995) 1 – 19. doi:10.1006/jcph.1995.1039.
- [40] E. B. Tadmor, R. E. Miller, *Modeling Materials: Continuum, Atomistic and Multiscale Techniques*, Cambridge University Press, 2011.
- [41] C. A. Becker, F. Tavazza, Z. T. Trautt, R. A. B. de Macedo, Considerations for choosing and using force fields and interatomic potentials in materials science and engineering - <http://www.ctcms.nist.gov/potentials>, *Current Opinion in Solid State and Materials Science* 17 (6) (2013) 277 – 283, *frontiers in Methods for Materials Simulations*. doi:10.1016/j.cossms.2013.10.001.
- [42] M. Maździarz, T. D. Young, P. Dłuzewski, T. Wejrzanowski, K. J. Kurzydłowski, Computer modelling of nanoindentation in the limits of a coupled molecular–statics and elastic scheme, *Journal of Computational and Theoretical Nanoscience* 7 (6) (2010) 1172 – 1181. doi:10.1166/jctn.2010.1469.
- [43] M. Maździarz, T. D. Young, G. Jurczak, A study of the affect of prereduction on the nanoindentation process of crystalline copper, *Archives of Mechanics* 63 (5-6) (2011) 533, <http://am.ippt.pan.pl/am/article/view/v63p533>.
- [44] A. Stukowski, Visualization and analysis of atomistic simulation data with OVITO-the Open Visualization Tool, *Modelling and Simulation in Materials Science and Engineering* 18 (1) (2010) 015012, <https://ovito.org/>. doi:10.1088/0965-0393/18/1/015012.
- [45] P. Hirel, AtomsK: A tool for manipulating and converting atomic data files, *Computer Physics Communications* 197 (2015) 212 – 219, <http://atomsk.univ-lille1.fr/index.php>. doi:10.1016/j.cpc.2015.07.012.

- [46] M. Maździarz, M. Gajewski, Estimation of Isotropic Hyperelasticity Constitutive Models to Approximate the Atomistic Simulation Data for Aluminium and Tungsten Monocrystals, *Computer Modeling in Engineering & Sciences* 105 (2) (2015) 123–150. doi:10.3970/cmes.2015.105.123.
- [47] G. Jurczak, M. Maździarz, P. Dłużewski, G. P. Dimitrakopoulos, P. Komninou, T. Karakostas, On the applicability of elastic model to very thin crystalline layers, *Journal of Physics: Conference Series* 1190 (2019) 012017. doi:10.1088/1742-6596/1190/1/012017.
- [48] Y. Mishin, M. J. Mehl, D. A. Papaconstantopoulos, A. F. Voter, J. D. Kress, Structural stability and lattice defects in copper: *Ab initio*, tight-binding, and embedded-atom calculations, *Phys. Rev. B* 63 (2001) 224106. doi:10.1103/PhysRevB.63.224106.
- [49] Y. Mishin, D. Farkas, M. J. Mehl, D. A. Papaconstantopoulos, Interatomic potentials for monoatomic metals from experimental data and *ab initio* calculations, *Phys. Rev. B* 59 (1999) 3393–3407. doi:10.1103/PhysRevB.59.3393.
- [50] M. Mendeleev, M. Kramer, S. Hao, K. Ho, C. Wang, Development of interatomic potentials appropriate for simulation of liquid and glass properties of NiZr₂ alloy, *Philosophical Magazine* 92 (35) (2012) 4454–4469. doi:10.1080/14786435.2012.712220.
- [51] M.-C. Marinica, L. Ventelon, M. R. Gilbert, L. Proville, S. L. Dudarev, J. Marian, G. Bencteux, F. Willaime, Interatomic potentials for modelling radiation defects and dislocations in tungsten, *Journal of Physics: Condensed Matter* 25 (39) (2013) 395502. doi:10.1088/0953-8984/25/39/395502.
- [52] X. W. Zhou, R. A. Johnson, H. N. G. Wadley, Misfit-energy-increasing dislocations in vapor-deposited CoFe/NiFe multilayers, *Phys. Rev. B* 69 (2004) 144113. doi:10.1103/PhysRevB.69.144113.
- [53] S. R. Wilson, K. G. S. H. Gunawardana, M. I. Mendeleev, Solid-liquid interface free energies of pure bcc metals and B2 phases, *The Journal of Chemical Physics* 142 (13) (2015) 134705. doi:10.1063/1.4916741.
- [54] M. R. Fellinger, H. Park, J. W. Wilkins, Force-matched embedded-atom method potential for niobium, *Phys. Rev. B* 81 (2010) 144119. doi:10.1103/PhysRevB.81.144119.
- [55] S. Han, L. A. Zepeda-Ruiz, G. J. Ackland, R. Car, D. J. Srolovitz, Interatomic potential for vanadium suitable for radiation damage simulations, *Journal of Applied Physics* 93 (6) (2003) 3328–3335. doi:10.1063/1.1555275.

- [56] B. Palosz, E. Grzanka, S. Gierlotka, S. Stel'makh, R. Pielaszek, U. Bismayer, J. Neufeind, H. Weber, T. Proffen, R. V. Dreele, W. Palosz, Analysis of short and long range atomic order in nanocrystalline diamonds with application of powder diffractometry, *Zeitschrift für Kristallographie* 217 (2002) 497–509. doi:10.1524/zkri.217.10.497.20795.
- [57] M. Moakher, N. Norris, The Closest Elastic Tensor of Arbitrary Symmetry to an Elasticity Tensor of Lower Symmetry, *J. Elasticity* 85 (2006) 215–263. doi:10.1007/s10659-006-9082-0.
- [58] K. Kowalczyk-Gajewska, Micromechanical model of polycrystalline materials with lamellar substructure, *Arch. Metal. Mater.* 56 (2011) 509–522. doi:10.2478/v10172-011-0055-3.
- [59] M. Haque, M. A. Saif, Mechanical behavior of 3050 nm thick aluminum films under uniaxial tension, *Scripta Materialia* 47 (12) (2002) 863 – 867. doi:10.1016/S1359-6462(02)00306-8.